Investigation of Novel Quinoline–Thiazole Derivatives as Antimicrobial Agents: *In Vitro* and *In Silico* Approaches

Asaf Evrim Evren,* Abdullah Burak Karaduman, Begüm Nurpelin Sağlik, Yusuf Özkay, and Leyla Yurttaş*

Cite This: *ACS Omega* 2023, 8, 1410–1429

Read Online

ACCESS | Metrics & More | Article Recommendations | Supporting Information

ABSTRACT: Infectious diseases are a major concern around the world. Today, it is an urgent need for new chemotherapeutics for infectious diseases. Because of that, our group designed, synthesized, and analyzed 14 new quinoline derivatives endowed with the pharmacophore moiety of fluoroquinolones primarily for their antimicrobial effects. Their cytotoxicity effects were tested against six bacterial and four fungal strains and NIH/3T3 cell line. Additionally, their action mechanisms were evaluated against DNA gyrase and lanosterol 14α-demethylase (LMD). Furthermore, to eliminate the potential side effects, the active compounds were evaluated against the aromatase enzyme. The experimental enzymatic results were evaluated for active compounds' binding modes using molecular docking and molecular dynamics simulation studies. The results were utilized to clarify the structure–activity relationship (SAR). Finally, compound **4m** was the most potent compound for its antifungal activity with low cytotoxicity against healthy cells and fewer possible side effects, while compounds **4j** and **4l** can be used alone for special patients who are suffering from fungal infections in addition to the primer disease.
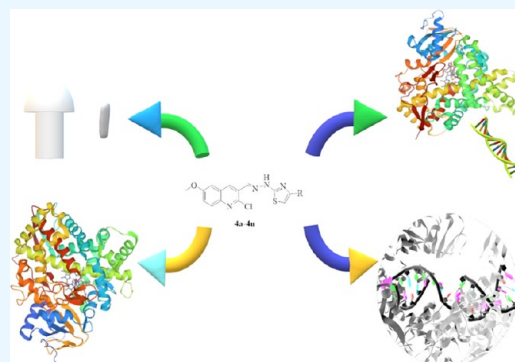
1. INTRODUCTION

Infection is described as pathogenic microorganisms' invasion and/or multiplying in the tissue or organ of another organism and then causing some undesirable effects in the host.[1,2] There are many pathogenic microorganisms like viruses, bacteria, fungi, yeast, *etc.* However, the incidence of bacterial and fungal infections is quite high worldwide than others.[3]

Although humanity has a symbiotic relationship with nonpathogenic bacteria and fungi, this relationship can be disrupted, and at this time, invasive microorganisms that can take advantage of this situation may cause infection.[4−7] They can also be contagious; various factors such as water, food, and travel play a role in the spread of these kinds of diseases.[8] In recent decades, resistance development is a major issue and is classified as drug-induced and microorganism-induced resistances. Mostly, they are related to unnecessary (incorrect dose or use of drugs in unrelated indications)[9] and multiple drug uses.[10−12] Additionally, misdiagnosis and wrong treatment methods,[13] prescriptions written only to eliminate symptoms (symptomatic treatment), or patients abandoning their treatment unfinished[14] make also some difficulties in the fighting against infectious diseases. Besides that, microbial infections are frequently seen in patients whose immune system is suppressed or insufficient, such as cancer and AIDS patients. In recent studies, the reported mortality and morbidity rates of microbial resistance developed by bacteria and fungi increased the

concerns,[15,16] especially regarding the inefficacy of the treatment applied in hospitals.[17]

Today, although the antimicrobial agents are classified depending on different properties such as action mechanism, spectrum width, and chemical structure, the structure–activity relationship (SAR) comes to the fore for medicinal chemists.[18] With the clinical use of nalidixic acid in 1964, scientists focused on the antimicrobial activity of quinoline derivatives.[19] Quinoline derivatives also play a role in cancer treatments (topoisomerase inhibition) due to their action mechanism (DNA-gyrase inhibition).[20−22] The structures of bacterial and eukaryotic topoisomerase IIs were identified, and they are highly similar to each other.[23] Even though this link seems satisfying, and the result may perceive as dual activity, they should be tested against healthy human cells in the current preclinical phase.

In addition, quinolones have a good antifungal activity profile[24−26] besides their antibacterial activity. Currently, the action mechanism of the drugs for the treatment of fungal diseases is generally based on blocking the ergosterol production because of their selectivity profile,[27,28] and with that, they break
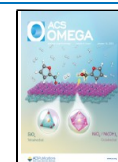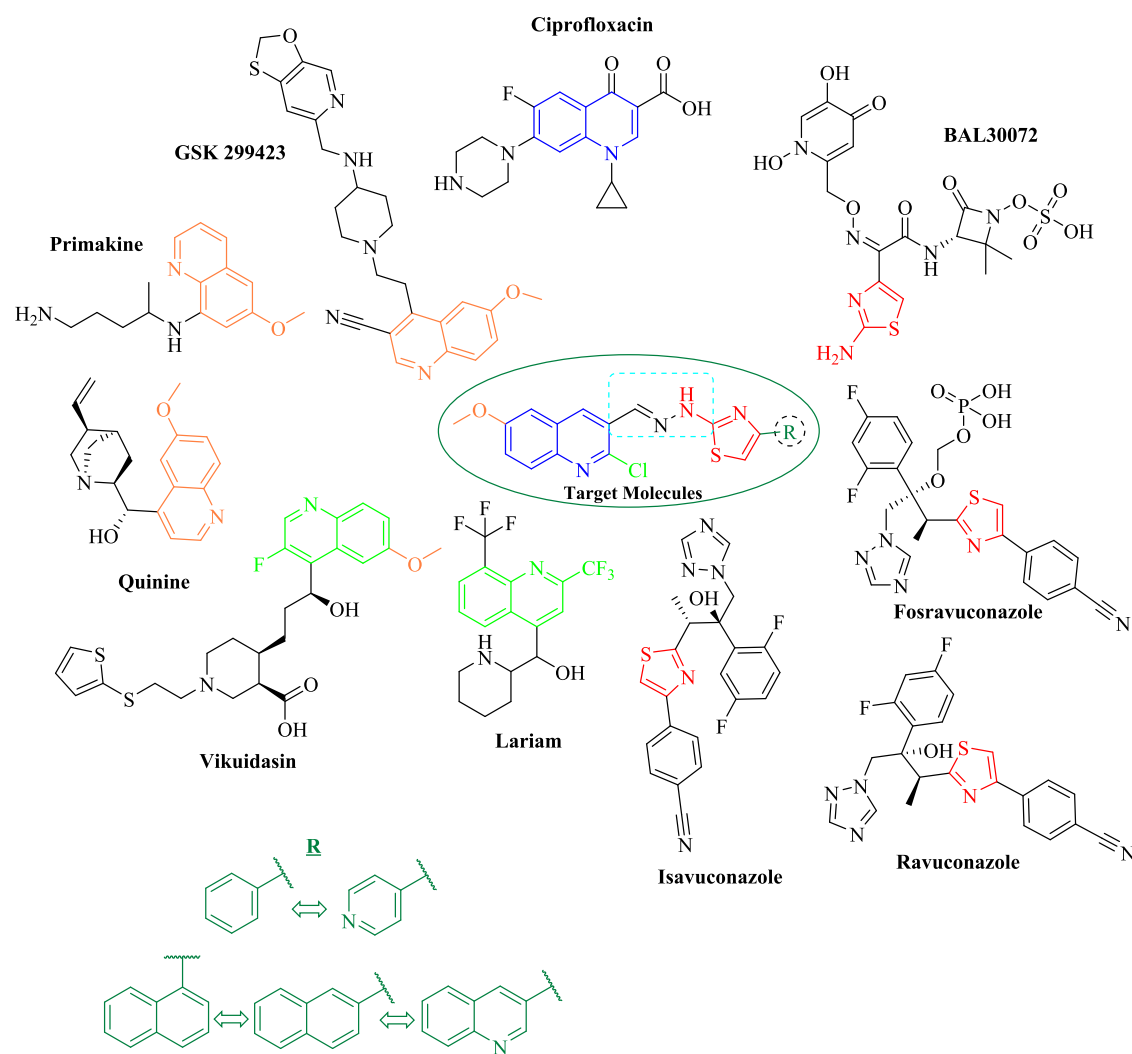
Figure 1. Designing the strategy of new quinoline derivatives as an antimicrobial agent. At the center of the figure, the target compounds are presented. Turquoise drawings schematize the analogue ring systems. Each color represents a moiety of target compounds.

the fungal cell integrity. The spectacular pathway for this activity is the inhibition of lanosterol 14α-demethylase (LDM).[29] Indeed, each antifungal imidazole analogue has previously been studied on P450, and they have been identified as potent ligands of the heme iron atom of P450s.[30] Moreover, ravuconazole and its analogues (fosravuconazole and isavuconazole) include a thiazole ring as a secondary azole, and albaconazole includes quinazolin-4-one ring, and their action mechanism is mediated through P450 enzymes.[31,32] Hence, it was proven that the other azole rings [such as (benzo)-1,2,3-triazole,[33,34] 1,2,4-triazole,[35,36] 1,3,4-oxadiazole,[37] and 1,3-thiazole] and non-azole nitrogen-rich rings may have also a good antifungal activity profile against invasive fungi. However, several side effects were reported,[38,39] probably caused by similarity to the human aromatase (HA) enzyme,[40] and also they showed some drug−drug interactions.[41] Hence, the design strategy should also involve inhibiting the LDM while not inhibiting HA.

Based on the above information, we designed, synthesized, and analyzed 14 new quinoline derivatives endowed with the pharmacophore moiety of fluoroquinolones to observe the antimicrobial effect. For this purpose, the literature knowledge was used to achieve a hybridization of the pharmacophoric groups of the molecules, as seen in Figure 1. The final molecules
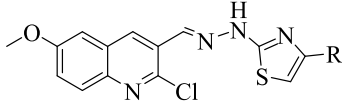
include 6-methoxy-2-chloroquinoline as the core structure. Their derivatization was achieved at the fourth position of the thiazole ring, and both aromatic ring systems were linked to each other with the hydrazone moiety. Their structure−activity relationship (SAR) and action mechanism were clarified *via in vitro* and *in silico* studies.

2. RESULTS AND DISCUSSION

2.1. Chemistry. The designed compounds (see Table 1) were synthesized and analyzed. The analyzed spectra are provided in the Supporting Information (Figures S1−S42).

2.1.1. ^{1}H NMR. Thiazole and quinoline are the common ring systems in all final compounds. In the sixth position of the quinoline, there is a methoxy and in the second position there is a chlorine substituent. Different aromatic substitutions were made at the fourth position of the thiazole ring, and the quinoline and the thiazole ring were linked by a hydrazone bridge. By investigating ^{1}H NMR spectra, the peak due to the fourth position proton of the quinoline was observed as a singlet between 8.68 and 8.78 ppm. The peak of hydrogen in the eighth position is observed as a doublet in the range of 7.82−7.91 ppm, and it is observed as a multiplet in some spectra because it is overlapped with other peaks. The peak due to the fourth position of the quinoline proton was observed as a doublet in the

Table 1. Synthesized Compounds

4a–4n

Compound	R	Compound	R
4a	---phenyl-F	4h	Cl-phenyl
4b	---phenyl-Cl	4i	O$_2$N-phenyl
4c	---phenyl-NO$_2$	4j	F-phenyl
4d	---phenyl	4k	O-phenyl
4e	---phenyl-CN	4l	N-pyridyl---
4f	---phenyl-CH$_3$	4m	naphthyl
4g	---phenyl-O	4n	naphthyl

Table 2. Antibacterial Activity Results of the Final Compounds (μg/mL)[a]

	A	B	C	D	E	F
4a	>1000	>1000	>1000	>1000	>1000	>1000
4b	>1000	>1000	>1000	>1000	>1000	>1000
4c	>1000	>1000	>1000	>1000	>1000	>1000
4d	>1000	>1000	>1000	>1000	>1000	>1000
4e	>1000	>1000	>1000	>1000	>1000	>1000
4f	>1000	>1000	>1000	>1000	>1000	>1000
4g	**7.81**	**3.91**	**7.81**	**3.91**	>1000	>1000
4h	>1000	>1000	>1000	>1000	>1000	>1000
4i	>1000	>1000	>1000	>1000	>1000	>1000
4j	>1000	>1000	>1000	>1000	>1000	>1000
4k	>1000	>1000	>1000	>1000	>1000	>1000
4l	>1000	>1000	>1000	>1000	>1000	>1000
4m	**7.81**	**7.81**	**7.81**	**7.81**	>1000	>1000
4n	>1000	>1000	**62.50**	>1000	>1000	>1000
RF-1	31.25	15.63	≤1.95	31.25	31.25	31.25
RF-2	≤1.95	≤1.95	≤1.95	3.91	≤1.95	≤1.95

[a]RF-1: chloramphenicol, RF-2: ciprofloxacin, A: *Escherichia coli* ATCC 35218, B: *E. coli* ATCC 25922, C: *Staphylococcus aureus* ATCC 6538, D: methicillin-resistant *S. aureus* (MRSA) (clinical isolate), E: *Salmonella typhimurium* ATCC 13311, F: *Klebsiella pneumoniae* NCTC 9633. Most active compounds are highlighted in red and moderately active compounds are written in bold.

range of 7.58−7.68 ppm because of the surrounding proton interactions. The peak due to the seventh position of the quinoline was observed in the 7.42−7.52 ppm range as doublets due to the surrounding proton interactions, and as multiplet, because it was partially overlapped with other peaks. The proton peak at the fifth position of the thiazole ring was observed generally as a singlet between 7.21 and 7.81 ppm, and multiplet was obtained since it was partially overlapped with other proton peaks. The two hydrogens, at the second and sixth positions of the 1,4-substituted phenyl derivatives (4a−c and 4e−g), were observed as doublets between 7.75 and 8.27 ppm, while the other two protons of the third and fifth positions were observed overlapped and as doublets between 6.97 and 8.11 ppm. Hydrogens of 3-substituted phenyl derivatives (4h−k) were obtained in the range of 6.87−8.65 ppm. According to the literature, the protons of the 4-substituted phenyl ring, 3-substituted phenyl ring, and mono-substituted phenyl ring follow the X$_2$Y$_2$, XYZW, and X$_2$Y$_2$Z spin systems, respectively. Although the cleavage patterns of the protons of the 1,4-disubstituted phenyl ring are mostly observed as two doublets (one for positions 2 and 6, one for positions 3 and 5), they can also be observed as singlet and quartet due to the properties of the substitutions.[42−44] Although proton cleavages of the 1,3-disubstituted phenyl ring are generally observed as one triplet (fifth position), two doublets (fourth and sixth positions), and one singlet (second position), very different cleavages can be observed due to the substitutions.[43,45]

The protons of the methylidene hydrazine (−HC=N−NH−) structure, which is common in all compounds, are generally singlet in the range of 8.41−8.49 ppm and partially multiplet due to mixing with other peaks; nitrogen proton was obtained as a broad singlet between 12.56 and 12.73 ppm. In the literature, they were observed as singlet and broad singlet.[43,46] When similar molecules were examined in the literature,[47] it was determined experimentally that compounds with a singlet peak at about 8.50 ppm were *E* isomers. This finding is suggested in this direction in terms of stability due to the presence of bulky groups in the structure of the compound.

In conclusion, the ^{1}H NMR data of all synthesized compounds were found to be consistent with the literature data.

2.1.2. ^{13}C NMR. According to the ^{13}C NMR data of the synthesized compounds, peaks were observed as expected. The common carbons' peaks and the unique carbons' peaks of the compounds were examined. Since compounds 4a and 4j contain fluorine as a substituent, the spectra of these compounds were obtained as one additional peak, as mentioned in the literature due to C−F cleavages.[48] The peaks of the carbon due to methylidene hydrazine, which is a common carbon for all compounds, were obtained in the range of 143.23−143.82 ppm similar to the literature.[46] Aromatic carbons peaked in the range of 102.64−168.62 ppm, and methoxy carbons were seen between 55.55 and 56.24 ppm.

Table 3. Anticandidal Activity Results of the Final Compounds (μg/mL)^a

	A	B	C	D		A	B	C	D
4a	>1000	1.95	31.25	15.63	**4h**	>1000	31.25	**≤0.06**	125
4b	>1000	**≤0.06**	31.25	31.25	**4i**	1.95	1.95	1.95	1.95
4c	>1000	62.50	31.25	31.25	**4j**	>1000	>1000	62.50	**≤0.06**
4d	1.95	1.95	1.95	15.63	**4k**	1.95	1.95	1.95	1.95
4e	3.91	**≤0.06**	62.50	3.91	**4l**	1.95	1.95	>1000	1.95
4f	>1000	**≤0.06**	3.91	3.91	**4m**	1.95	1.95	**≤0.06**	**0.24**
4g	>1000	15.63	31.25	3.91	**4n**	3.91	1.95	1.95	1.95
Rf	≤0.06	0.24	≤0.06	≤0.06					

^{a}RF: ketoconazole, A: *Candida albicans* ATCC 24433, B: *C. glabrata* ATCC 90030, C: *Candida krusei* ATCC 6258, D: *Candida parapsilosis* ATCC 22019. Most active compounds are highlighted in red and moderately active compounds are written in bold.

Table 4. IC$_{50}$ (μM) of the Compounds against NIH/3T3 Cells

compound	IC$_{50}$ ± STD	compound	IC$_{50}$ ± STD
4a	39.83 ± 1.45	**4h**	14.48 ± 0.57
4b	14.72 ± 0.34	**4i**	8.54 ± 0.26
4c	31.60 ± 0.87	**4j**	10.00 ± 0.39
4d	1.26 ± 0.033	**4k**	12.04 ± 0.44
4e	>1000	**4l**	>1000
4f	>1000	**4m**	34.51 ± 0.88
4g	10.40 ± 0.22	**4n**	>1000

2.1.3. High-Resolution Mass Spectrum. Mass spectra of the final compounds were obtained using the electrospray ionization (ESI) technique.[43] When the mass spectra were examined, M + 1 peaks were detected in all compounds (**4a−n**).

2.2. Results of Antibacterial Tests. Interestingly, no antibacterial effect was observed in compounds other than **4g**, **4m**, and **4n**. However, when the antibacterial activities of these three compounds, especially **4g** and **4m**, were compared with the antibacterial effects of ciprofloxacin and chloramphenicol, they have a good antibacterial profile. Results of the antibacterial activity are shown in Table 2.

Minimum inhibitory concentrations (MIC$_{90}$) of chloramphenicol, which inhibit 90% of the microbial population, were determined as 31.25 and 15.63 μg/mL against *E. coli* (ATCC 35218) and *E. coli* (ATCC 25922) strains, respectively. On the other hand, the MIC$_{90}$ of ciprofloxacin was found to be lower than 1.95 μg/mL. Therefore, it was concluded that compound **4g** (MIC$_{90}$: 7.81; 3.91 μg/mL) was four times more effective against both *E. coli* strains (ATCC 35218; ATCC 25922) than chloramphenicol. Like **4g**, compound **4m** (MIC$_{90}$: 7.81; 7.81 μg/mL) was four times more effective against *E. coli* (ATCC
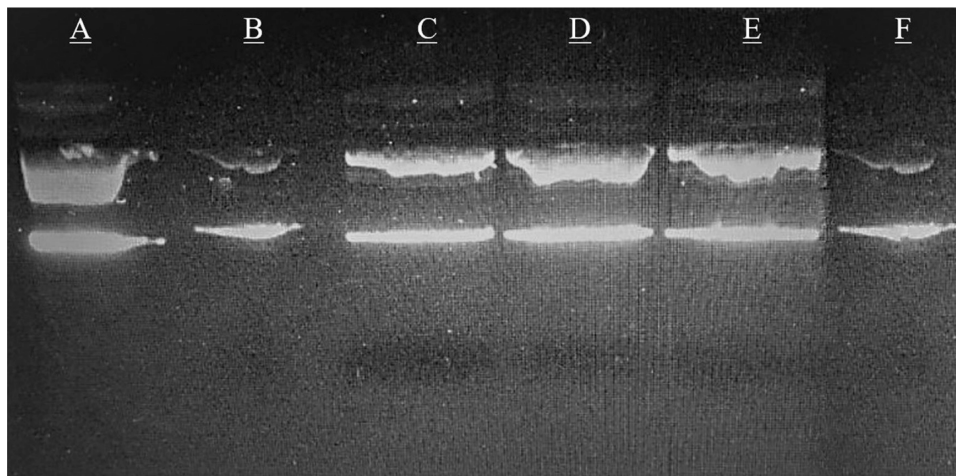

Figure 2. Inhibition visualities of compounds **4g** and **4m** and ciprofloxacin against *E. coli* DNA gyrase by electrophoresis. (A) Relax (pHOT1) DNA image: no chemicals and DNA gyrase; (B) supercoiled DNA image: relaxed (pHOT1) DNA with gyrase, no chemicals; (C) compound **4g**: relax (pHOT1) DNA, gyrase, and chemical dissolved in dimethyl sulfoxide (DMSO); (D) compound 4m: relax (pHOT1) has DNA, gyrase, and chemical dissolved in DMSO, (E) positive control: there is relax (pHOT1) DNA, gyrase, and ciprofloxacin dissolved in DMSO; and (F) negative control: there is relax (pHOT1) DNA, gyrase, and DMSO only.

Table 5. CYP51A1 Inhibition% Results of the Final Compounds (μg/mL)

| | C. glabrata | | | |
| | concentrations (μg/mL) | | | |
compounds	3.91	0.98	0.24	0.06
4b	70.345 ± 2.638	60.197 ± 2.095	51.754 ± 1.612	36.198 ± 0.965
4e	25.398 ± 0.832	21.721 ± 0.955	18.289 ± 0.785	16.680 ± 0.774
4f	79.524 ± 2.141	65.073 ± 1.676	53.774 ± 2.390	42.132 ± 1.561
ketoconazole	89.368 ± 3.236	72.768 ± 2.868	61.856 ± 1.833	50.422 ± 1.162
fluconazole	86.512 ± 2.752	70.144 ± 2.052	63.679 ± 2.185	46.267 ± 0.936
	C. krusei			
	concentrations (μg/mL)			
compounds	3.91	0.98	0.24	0.06
4h	82.223 ± 2.575	67.651 ± 1.736	60.184 ± 1.985	45.530 ± 0.961
4i	20.021 ± 0.848	18.361 ± 0.767	14.178 ± 0.655	11.662 ± 0.479
4m	85.408 ± 3.502	70.574 ± 2.648	61.289 ± 1.461	48.431 ± 2.036
ketoconazole	87.657 ± 3.436	75.647 ± 2.749	60.630 ± 2.875	52.865 ± 1.662
fluconazole	85.168 ± 3.055	72.523 ± 1.961	60.132 ± 2.042	43.378 ± 0.937
	C. parapsilosis			
	concentrations (μg/mL)			
compounds	3.91	0.98	0.24	0.06
4j	75.164 ± 2.828	63.508 ± 1.948	55.281 ± 1.174	41.867 ± 0.968
4k	23.518 ± 1.051	17.437 ± 0.861	15.662 ± 0.616	11.449 ± 0.518
4l	78.667 ± 2.237	62.949 ± 2.626	56.137 ± 0.928	40.328 ± 1.326
ketoconazole	88.245 ± 2.662	71.864 ± 2.229	63.419 ± 2.074	55.348 ± 1.091
fluconazole	87.786 ± 3.147	73.204 ± 2.031	61.533 ± 1.282	49.579 ± 1.733

Table 6. Aromatase IC_{50} Results of the Final Compounds (μM)

compound		compound	
4i	0.033 ± 0.001	**4k**	0.038 ± 0.001
4j	0.047 ± 0.001	**4l**	0.042 ± 0.002
letrozole	0.026 ± 0.001		

35218) and twice as effective against *E. coli* (ATCC 25922). The MIC_{90} values of chloramphenicol against *S. aureus* (ATCC 6538) and methicillin-resistant *S. aureus* (MRSA) (clinical isolate) strains were ≤1.95 and 31.25 μg/mL, respectively. According to these findings, compound **4g** (MIC_{90}: 3.91 μg/mL) was 8 times more effective than the standard drug against methicillin-resistant *S. aureus* (MRSA) (clinical isolate), while compound **4m** (MIC_{90}: 7.81 μg/mL) was 4 times more effective.

Table 7. Physicochemical, Pharmacokinetic, and Pharmaceutical Chemistry Properties of the Synthesized Compounds[a]

	PP			pharmacokinetic properties				PC	
	HBA	HBD	TPSA	Log P	Log S	MBE	Log K_p	LK	SK
4a	5	1	87.64	4.97	−7.48	high	−4.65		3.17
4b	4	1	87.64	5.19	−8.02	high	−4.38		3.18
4c	6	1	133.46	3.91	−8.15	low	−5.01		3.25
4d	4	1	87.64	4.65	−7.38	high	−4.61		3.16
4e	5	1	111.43	4.44	−7.58	high	−4.97		3.26
4f	4	1	87.64	4.99	−7.75	high	−4.44		3.28
4g	5	1	96.87	4.65	−7.54	high	−4.82		3.31
4h	4	1	87.64	5.19	−8.02	high	−4.38		3.17
4i	6	1	133.46	3.98	−8.15	low	−5.01		3.31
4j	5	1	87.64	4.98	−7.48	high	−4.65		3.17
4k	5	1	96.87	4.66	−7.54	high	−4.82		3.34
4l	5	1	100.53	3.92	−6.54	high	−5.38		3.11
4m	4	1	87.64	5.54	−8.68	low	−4.03		3.38
4n	4	1	87.64	5.55	−8.68	low	−4.03		3.38
RD_1	5	2	74.57	1.10	0.00	high	−9.09		2.51
RD_2	5	0	69.06	3.55	−5.51	high	−6.46	+(1)	4.45

[a]PP: physicochemical properties, HBA: number of hydrogen bond acceptor, HBD: number of hydrogen bond donor, TPSA: topological polar surface area ($Å^2$), Log P: partition coefficient, Log S: solubility coefficient in water, MBE: absorption level by the gastrointestinal system, Log K_p: skin absorption coefficient (cm/sn), PC: pharmaceutical chemistry; LK: violation number of rule of five, SK: synthesis ease score in terms of medicinal chemistry (1: very easy, 10: very hard, r^2: 0.94), RD_1: reference drug-1 (ciprofloxacin), RF_2: reference drug-2 (ketoconazole).
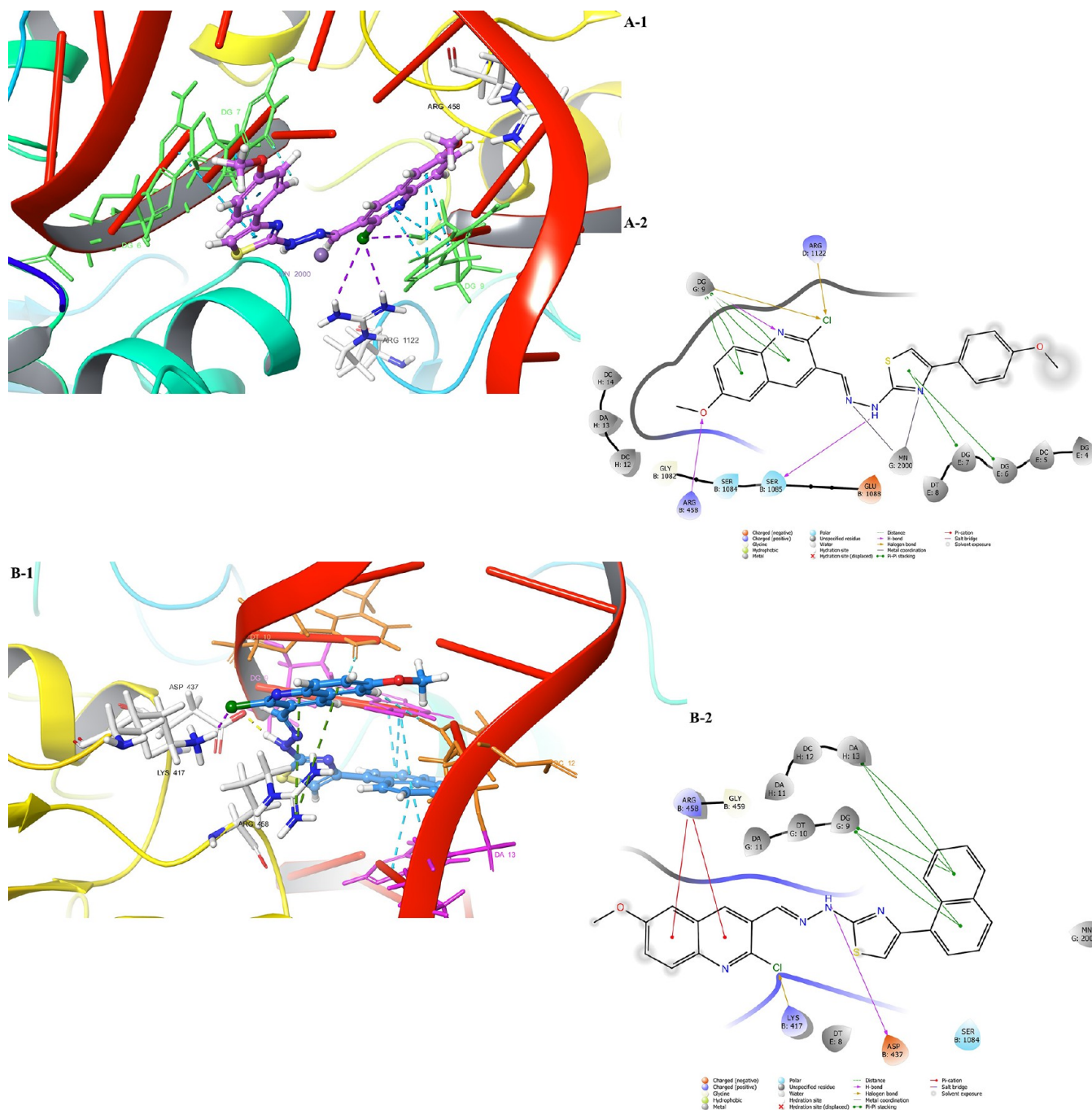
Figure 3. Docking poses of the antibacterial active compounds in the active side of DNA gyrase (PDB ID: 2XCT). 2D and 3D poses of the compounds are viewed. (A) Compound **4g** and (B) compound **4m**. Nucleotides are represented by the residue-type color. For clarity, only interacted residues are viewed.

Compounds **4g**, **4m**, and **4n** showed significant antibacterial activity against *S. aureus* (ATCC 6538) strain at 7.81, 7.81, and 62.50 μg/mL, respectively.

The synthesized compounds (**4a–n**) did not show antibacterial activity against *S. typhimurium* (ATCC 13311) and *K. pneumoniae* (NCTC 9633) strains.

2.3. Results of Antifungal Tests. Ketoconazole was used as the reference drug to evaluate the anticandidal activities of the final compounds. Its MIC_{90} values were determined as 0.24 μg/mL against *Candida glabrata* (ATCC 90030) and less than 0.06 μg/mL for other species. Results of the antifungal activity are shown in Table 3.

Compounds **4d**, **4i**, **4k**, **4l**, and **4m** were more effective than other derivatives against *C. albicans* (ATCC 24433). The MIC_{90} value of these five compounds was 1.95 μg/mL, and the MIC_{90} value of compounds **4e** and **4n** was determined as 3.91 μg/mL. The other analogues did not show anticandidal activity.

All compounds except **4j** showed cytotoxicity against *C. glabrata* (ATCC 90030). Compounds **4b**, **4e**, and **4f** showed extraordinary anticandidal activity when compared with other analogues and ketoconazole. Their MIC_{90} values were determined less than 0.06 μg/mL. Besides that, the MIC_{90} values of compounds **4a**, **4d**, **4i**, and **4k–n** were 1.95 μg/mL. The anticandidal activity against *C. glabrata* (ATCC 90030) was

Table 8. Interaction Index for the Active Compounds—DNA-Gyrase Enzyme Complex

compound	ligand moiety	residue	interaction type, count
4g	oxygen of quinoline methoxy	chain B: Arg458	1 H-bond
	N_2 of hydrazone	Ser1085	1 H-bond
	chlorine of quinoline	chain D: Arg1122	1 halogen bond
	thiazole ring	chain E: DG6	1 π–π stacking
	thiazole ring	DG7	1 π–π stacking
	N of quinoline ring	chain G: DG9	1 H-bond
	chlorine of quinoline	DG9	1 halogen bond
	quinoline ring	DG9	4 π–π stackings
	N_1 of hydrazone	Mn2000	1 metal chelate
	N of thiazole	Mn2000	1 metal chelate
4m	chlorine of quinoline	chain B: Lys417	1 halogen bond
	N_1 of hydrazone	Asp437	1 H-bond
	quinoline ring	Arg458	2 π–cation interactions
	naphthalene ring	chain G: DG9	3 π–π stackings
	naphthalene ring	chain H: DA13	2 π–π stackings

seen at 15.63 μg/mL for **4g**, at 31.25 μg/mL for **4h**, and 62.50 μg/mL for **4c**.

The MIC$_{90}$ values of **4h** and **4m** against *C. krusei* (ATCC 6258) were ≤0.06 μg/mL. However, the MIC$_{90}$ values of compounds **4d**, **4i**, **4k**, and **4n** were 1.95 μg/mL, 3.91 μg/mL for **4f**, 31.25 μg/mL for **4a**−**c** and **4g**; and 62.50 μg/mL for **4e** and **4j**. Despite the very high cytotoxicity of the 13 derivatives, compound **4l** did not show cytotoxicity.

All compounds have anticandidal effects against *C. parapsilosis* (ATCC 22019) compared to other *Candida* species. In particular, compound **4j** has even higher efficacy on *C. parapsilosis* (ATCC 22019) than the reference drug, although it did not show activity against *C. albicans* (ATCC 24433) and *C. glabrata* (ATCC 90030) cells. The MIC$_{90}$ value of **4j** was less than 0.06 μg/mL. In addition, compound **4m** (MIC$_{90}$: 0.24 μg/mL) showed significant cytotoxicity against other *Candida* species.

As a result, compounds **4d**, **4e**, **4i**, **4k**, **4m**, and **4n** showed anticandidal activity at very low concentrations against all *Candida*. Specifically, the chlorine (**4b**, **4h**) substitution at the para or meta positions, the cyano group (**4e**) at the para position, the methyl group (**4f**) at the meta position, the flour atom (**4j**) at the meta position of the phenyl ring, or naphthalene-1-yl (**4m**) substitution were marked as remarkable derivatives.

Antifungal activity against *C. albicans* (ATCC 24433) did not increase, even more, and disappeared in the presence of substitution on the phenyl ring. The anticandidal activity was preserved when pyridine or naphthalene was substituted instead of the phenyl derivatives.

When phenyl was substituted at the meta position, anticandidal activity against *C. glabrata* (ATCC 90030) was preserved or disappeared. Furthermore, the substitutions of 4-Cl, 4-CN, or 4-CH$_3$ phenyl increased the activity tremendously. In both the third and fourth position substitutions, the electron-donating groups showed higher activity than the electron-withdrawing groups. It was observed that the activity was preserved in the replacement of phenyl with other rings. Compounds showing selectivity for this species were identified as **4b**, **4e**, and **4f**.

The effect of para substitution of the phenyl on the antifungal activity against *C. krusei* (ATCC 6258) resulted in decreased efficacy. In addition, the electron-donating groups showed higher activity than the electron-withdrawing groups similar to anti-*C. glabrata*. The activity vanished by replacing the phenyl with a pyridine, and in contrast, replacing the phenyl with a naphthalene-1-yl caused the activity to increase significantly. Furthermore, using naphthalene-2-yl instead of phenyl resulted in the activity being preserved. This strain was found to be sensitive to compounds **4h** and **4m**.

In the analysis of the anticandidal activity against *C. parapsilosis* (ATCC 22019), the presence of an electron-donating group at the para position of the phenyl ring was observed to increase the activity 4 times compared to the meta position substitutions. However, 3- or 4-chloro substitution on the phenyl reduces the activity. If the group or atom could make a hydrogen bond and it is at the third position of the phenyl, then it could increase the activity 8-fold; otherwise, the activity decreases 8-fold. Otherwise, if the substitutions could form the hydrogen bond, then the activity of these substitutions could be 64 times more than other substitutions. Besides that, replacing the phenyl ring with a pyridine and naphthalene-2-yl moieties or with naphthalene-1-yl moiety increased the activity 8 times or 64 times, respectively. Compound **4j** was identified as a selective molecule for this species.

When the results were evaluated for all fungi species, it was determined that there was no difference between the electron-donating or -withdrawing substituents. Moreover, compounds (**4i** and **4k**) having 3-NO$_2$ and 3-OCH$_3$ groups showed similar anticandidal activity at the same concentrations against all fungi species. Naphthalen-1-yl substitution (**4m**) was determined as the most active compound against all fungal cells.

2.4. Results of Cytotoxic Effects on NIH/3T3 Cell Line. The cytotoxicity effect of the compounds was tested against NIH/3T3 healthy cell line and determined as IC$_{50}$ (μM) (displayed in Table 4).

The results can be sorted from the most cytotoxic to the less cytotoxic compounds as **4d** > **4i** > **4j** > **4g** > **4k** > **4h** > **4b** > **4c** > **4m** > **4e** = **4f** = **4l** = **4n** against the NIH/3T3 healthy cell line. In fact, except for compound **4d**, it can be suggested that all compounds were found safe considering that their MIC$_{90}$/IC$_{50}$ ratio is less than 1. Moreover, IC$_{50}$ values of compounds **4e**, **4f**, **4l**, and **4n** were higher than 1000 μM.

2.5. Results of Enzyme Inhibition Tests. *2.5.1. DNA-Gyrase Enzyme Inhibition.* The inhibition activity on the DNA-gyrase enzyme was performed *via* an electrophoretic method for ciprofloxacin, compounds **4g** and **4m**. The obtained results are displayed in Figure 2.

In the figure, the reference drug and the synthesized compounds have very similar appearances, and there was no peak belonging to the supercoiled DNA. Thus, it can be concluded that the antibacterial effect of compounds **4g** and **4m** was caused by the inhibition of the DNA-gyrase enzyme.

2.5.2. Lanosterol 14α-Demethylase (LMD, CYP51A1) Inhibition Tests. The activity of the target compounds was tested against *Candida* strains *via* the determination of ergosterol production. The results are shown in Table 5.

The test results showed that the activation mechanism of some active compounds (**4b**, **4f**, **4h**, **4j**, **4l**, and **4m**) was achieved *via* blocking ergosterol production, which eventually ruins the cell integrity. The fact that compounds **4e**, **4i**, and **4k** did not decrease the ergosterol production compared to the standard drugs led to the conclusion that their antifungal activity
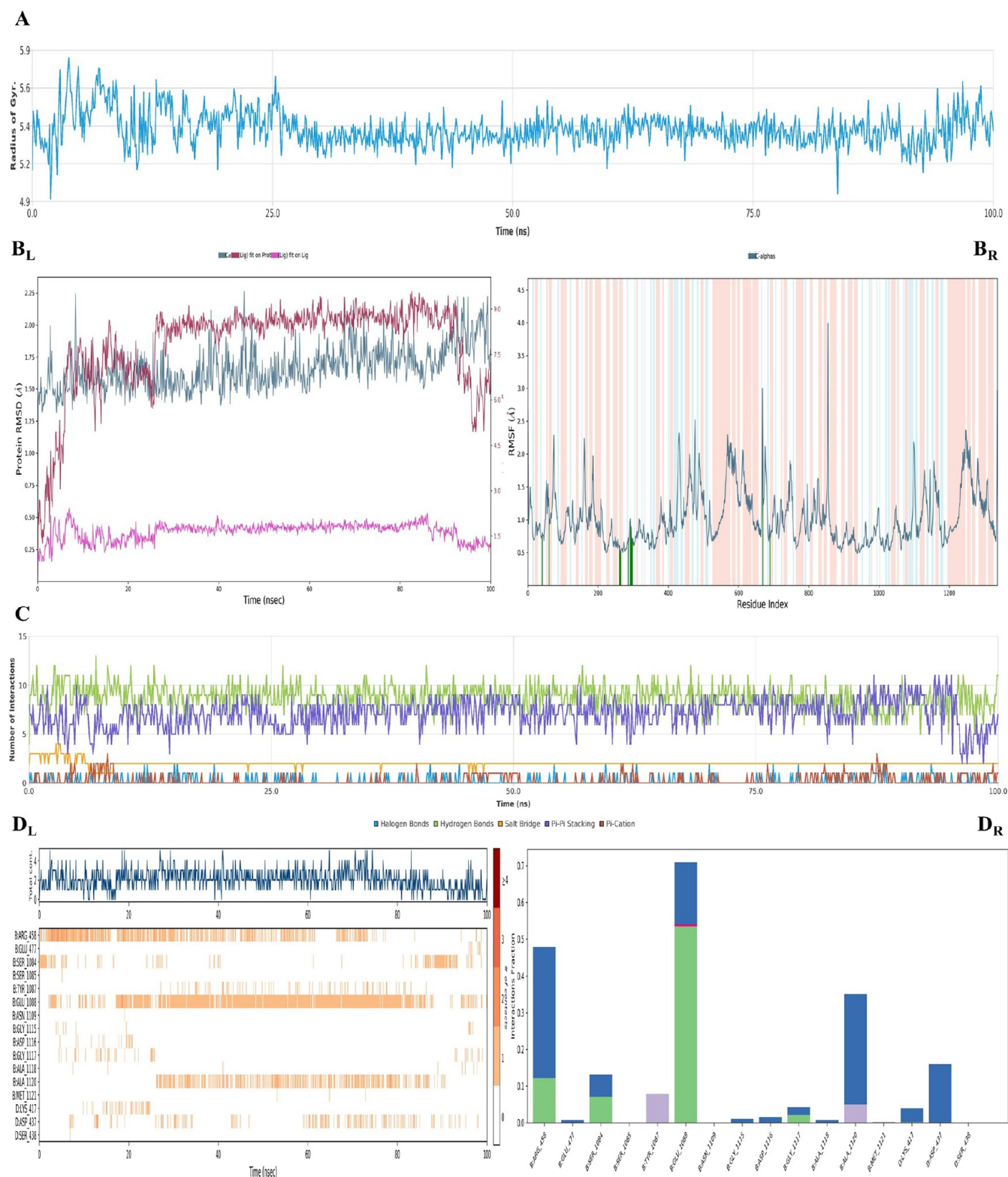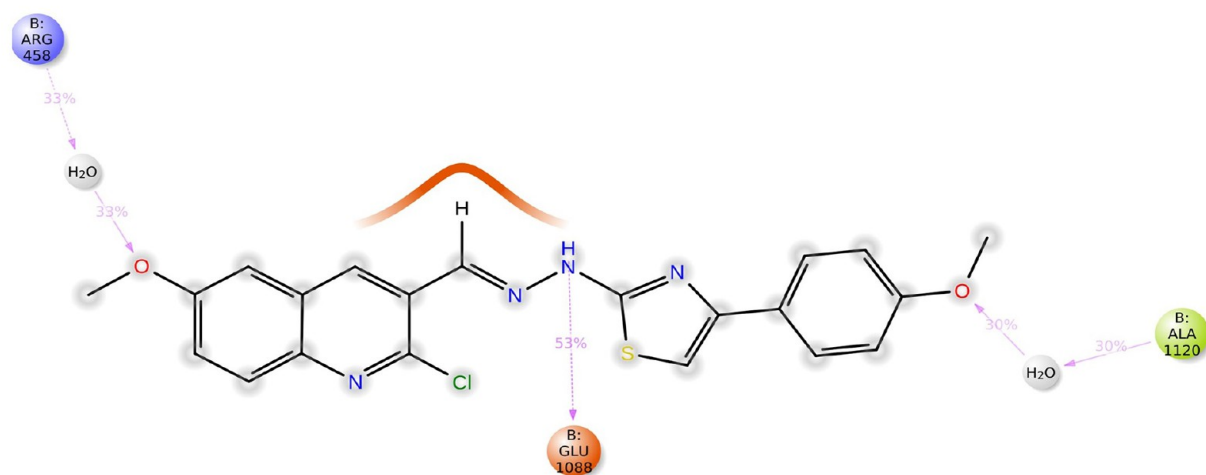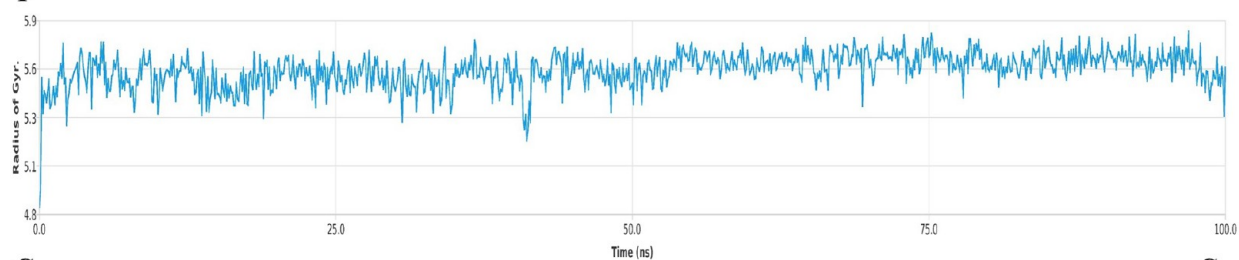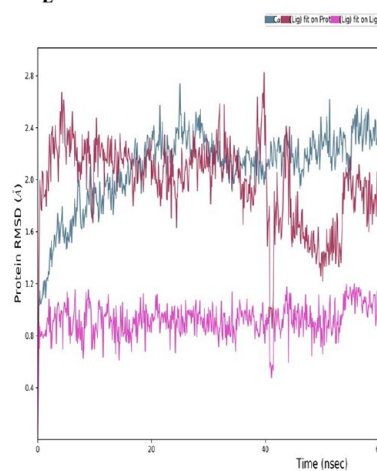
A

B$_L$

B$_R$

C

D$_L$

D$_R$

Figure 4. continued

E

F

G$_L$ **G$_R$**
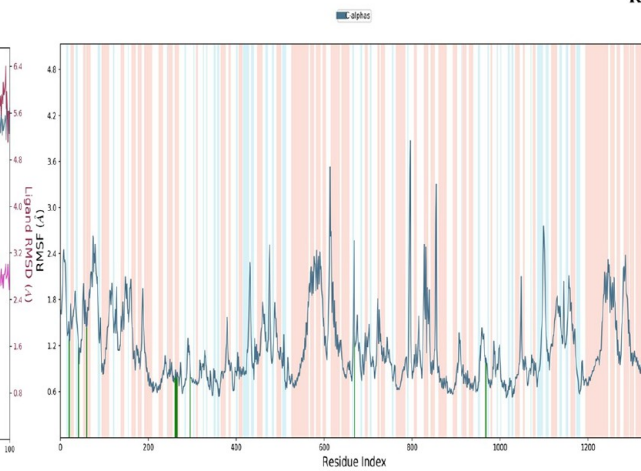
H

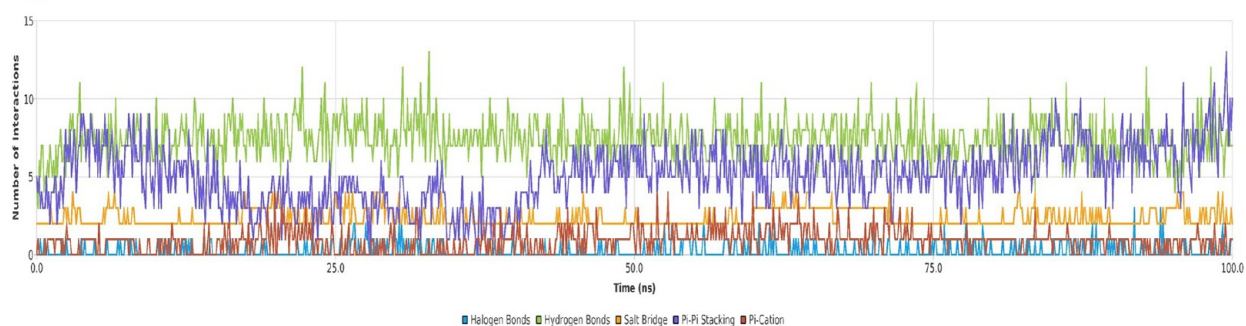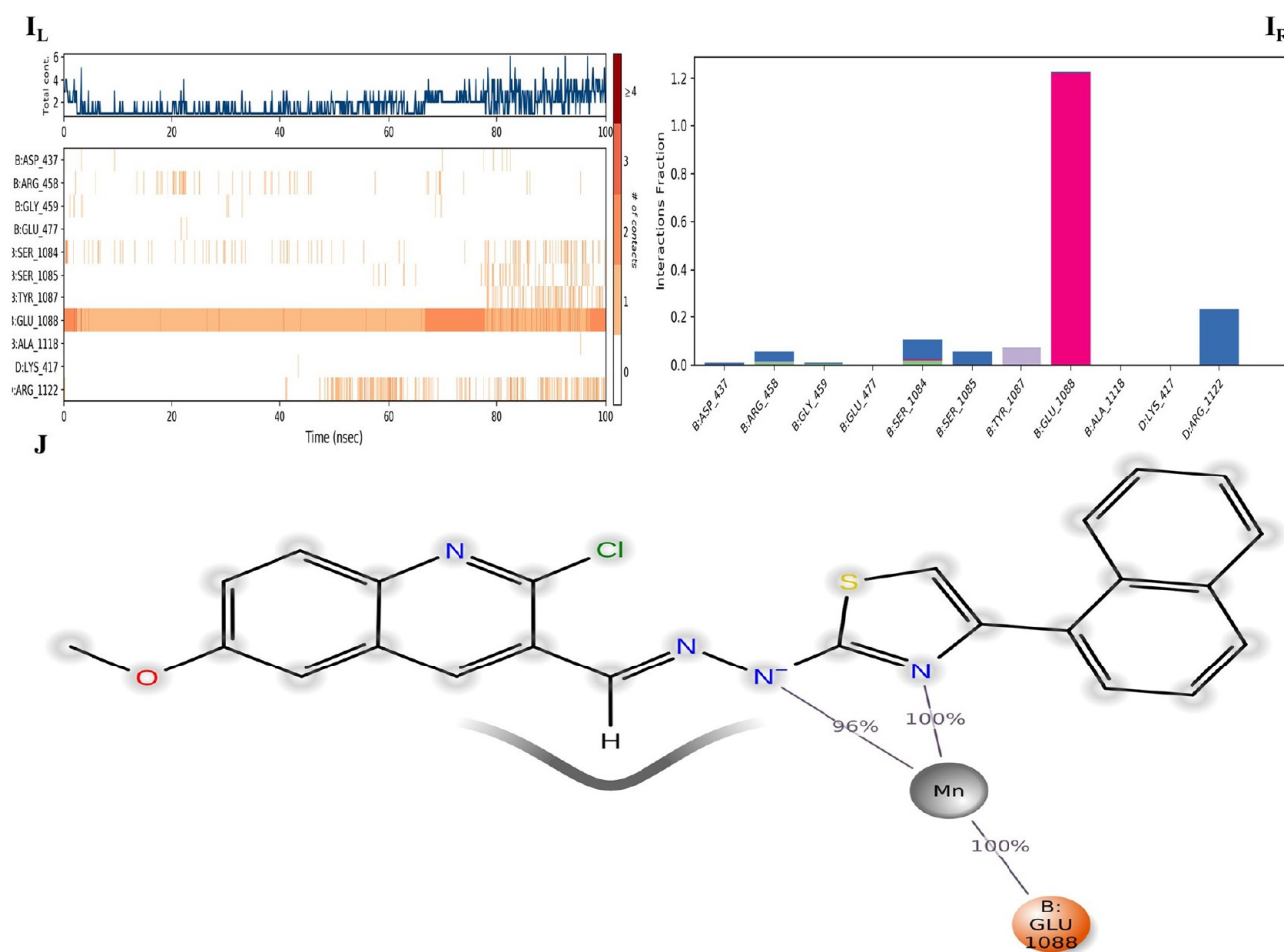**Figure 4.** continued

Figure 4. Plots of the MDS results for **4g**− and **4m**−DNA−DNA-gyrase complexes. The stability properties (R_g, root-mean-square deviation (RMSD), and root-mean-square fluctuation (RMSF) plots, respectively) are shown in (A), (B), (F), and (G) sections. The interaction properties ((C, H) number of interactions−interaction types−time plot; (D_R, I_R) interaction fraction−residue diagram; (D_L, I_L) total connections−residues−time plot; (E, J) 2D interaction pose with connection strength (cutoff = 0.2) at the active region) are in (C)−(E) and (H)−(J) sections, respectively.

does not occur *via* inhibition of the LMD enzyme. As a result, we determined that even though all compounds did not show their antifungal activity *via* LMD enzyme inhibition, the active compounds (**4b**, **4f**, **4h**, **4j**, **4l**, and **4m**) showed their anticandidal activity *via* LMD enzyme inhibition. For the next study, we aimed the determination of the antifungal mechanism of compounds **4e**, **4i**, and **4k**.

2.5.3. Human Aromatase (HA) Inhibition. It was mentioned in the Introduction section that antifungal agents acting *via* a mechanism that involves the LDM pathway can cause some side effects. Thus, we aim to eliminate those possible side effects, so we also tested the antifungal active compounds on HA. The results are shared in Table 6. (Only compounds with inhibiting HA enzyme IC_{50} values were shared among antifungal active compounds.)

The IC_{50} values of the active compounds **4i**, **4j**, **4k**, and **4l** were 0.038, 0.042, 0.047, and 0.033 μM against aromatase enzyme, respectively. The IC_{50} values of these compounds were found very close to the standard drug (letrozole, 0.026 μM). The remaining active antifungal compounds did not show aromatase inhibition activity.

2.6. Results of *In Silico* Studies. *2.6.1. Results of ADME Parameters and Lipinski's Rule of Five.* The evaluation of some properties of the compounds and whether they violate Lipinski's rule of five are given in Table 7. This rule does not determine

whether the compounds are pharmacologically active but indicates that compounds that comply with the rule are less likely to be eliminated during clinical trials and thus have a better chance of reaching the market.

According to the results, the compounds are predicted to be suitable for oral use since the final molecules do not violate Lipinski's RoF. However, it was calculated that molecules carrying NO_2 phenyl or naphthalene moieties may have low absorption from the gastrointestinal tract. When the rates of compounds passing through the horny layer, known as the rate-limiting step, are evaluated for topical drug applications,[49] it is predicted that all compounds are suitable for that. The synthesis feasibility of the target compounds in terms of medicinal chemistry was determined as easy compared to that of ketoconazole and difficult compared to that of ciprofloxacin. In conclusion, the prediction results of the compounds suggest that they can be used for both oral and topical uses.

2.6.2. Binding Modes on DNA-Gyrase Enzyme and SAR. The best docking poses and their interaction indices are shared in Figure 3 and Table 8.

According to the literature,[50] the interactions with Arg458 and Asp437 amino acids have an important impact on the inhibition activity of DNA gyrase since those connections can stabilize both the DNA and gyrase enzyme; thus, the complex will not go under the supercoiled state. On the other hand, a
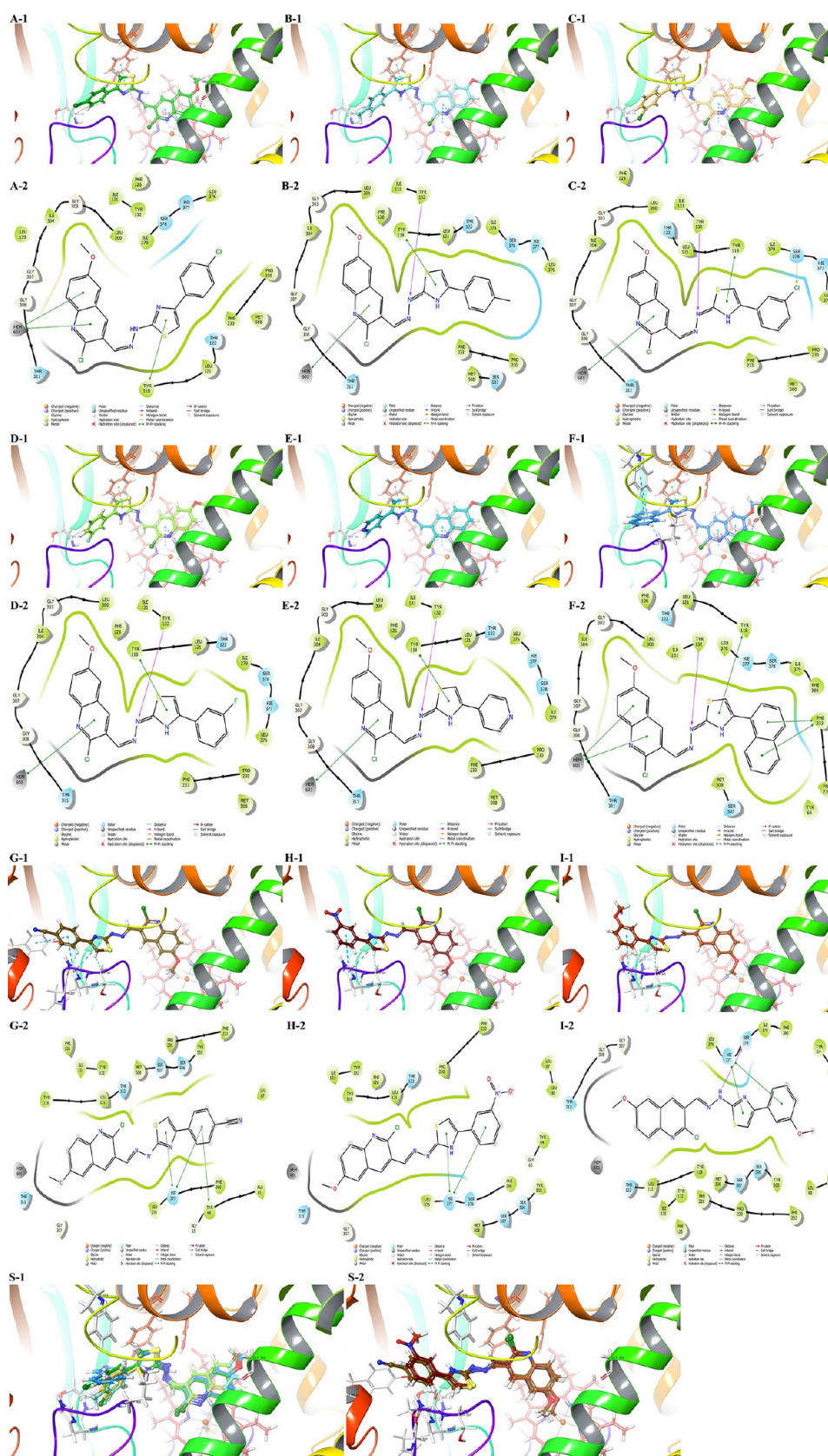
Figure 5. Docking poses of the antifungal active compounds in the active side of the LDM enzyme (PDB ID: 5TZ1). 2D and 3D poses of the compounds were viewed. (A) Compound **4b**; (B) compound **4f**; (C): compound (**4h**); (D) compound **4j**; (E) compound **4l**; (F) compound **4m**; (G) compound **4e**; (H) compound **4i**; and (I) compound **4k**. (S-1) 3D superimposed of the active compounds against the CYP51A1 enzyme; (S-2) 3D superimposed of the inactive compounds against the CYP51A1 enzyme.

Table 9. Interaction Index for the Active Compounds—Lanosterol 14α-Demethylase Enzyme Complex

compound	ligand moiety	residue	interaction type, count
4b	thiazole ring	Tyr118	1 π–π stacking
	H$_7$ of the quinoline ring	Gly303	1 ar H-bond
	H$_2$ of the phenyl ring	Ser378	1 ar H-bond
	quinoline ring	HEM601	2 π–π stackings
4f	thiazole ring	Tyr118	1 π–π stacking
	N$_1$ of hydrazone	Tyr132	1 H-bond
	H$_3$ of the phenyl ring	Ser378	1 ar H-bond
	quinoline ring	HEM601	2 π–π stackings
4h	thiazole ring	Tyr118	1 π–π stacking
	N$_1$ of hydrazone	Tyr132	1 H-bond
	Cl of the phenyl ring	Ser378	1 halogen bond
	quinoline ring	HEM601	2 π–π stackings
4j	thiazole ring	Tyr118	1 π–π stacking
	N$_1$ of hydrazone	Tyr132	1 H-bond
	H$_2$ of the phenyl ring	Ser378	1 ar H-bond
	quinoline ring	HEM601	2 π–π stackings
4l	thiazole ring	Tyr118	1 π–π stacking
	N$_1$ of hydrazone	Tyr132	1 H-bond
	H$_3$ of the phenyl ring	Ser378	1 ar H-bond
	quinoline ring	HEM601	2 π–π stackings
4m	thiazole ring	Tyr118	1 π–π stackings
	H$_2$ of the naphthalene ring	Tyr118	1 ar-H-bond
	N$_1$ of hydrazone	Tyr132	1 H-bond
	Naphthalene ring	Phe233	2 π–π stackings
	H$_7$ of the quinoline ring	Gly303	1 ar H-bond
	H$_7$ of the naphthalene ring	Met508	1 ar H-bond
	quinoline ring	HEM601	3 π–π stackings
4e	phenyl ring	Tyr64	1 π–π stacking
	phenyl ring	His377	1 π–π stacking
	thiazole ring	His377	1 π–π stacking
	H$_2$ of the phenyl ring	Ty505	1 ar H-bond
	H$_5$ of the thiazole ring	Ser507	1 ar H-bond
4i	phenyl ring	His377	1 1 π–π stacking
	thiazole ring	His377	1 π–π stacking
	H$_5$ of the thiazole ring	Ser507	1 ar H-bond
4k	phenyl ring	His377	1 1 π–π stacking
	thiazole ring	His377	1 π–π stacking
	N$_1$ of hydrazone	Ser378	1 ar H-bond
	H$_5$ of the thiazole ring	Ser507	1 ar H-bond

divalent metal atom (Mg^{2+}) is also important for DNA-gyrase activation since it is believed to be necessary to both cleave and re-ligate the DNA. In this study, both compounds interacted with Arg458, but only compound **4m** formed a H-bond with the Asp437 residue, and only compound **4g** was chelated with G:Mg2000. Therewithal, both compounds made hydrophobic interactions with different nucleotides (G:DG6, DG7, DG9, and H:DA13), but a common one was the DG9 nucleotide. Moreover, compound **4g** formed a H-bond with this nucleotide. All of these differences are probably caused by the hydrophobic part of the substituents. Because the naphthalene ring (**4m**) can interact with nucleotides *via* π–π stacking, it can most likely be easily localized. Besides that, the 4-methoxyphenyl moiety (**4g**) was under solvent exposition. In conclusion, both compounds showed interest in the DNA-gyrase complex differently, but they occupied the same pocket of the complex to bind. And these interactions are in harmony with the *in vitro* results.

To understand the effects of environmental changes and clarify SAR more specifically, the molecular dynamics

simulations (MDS) study was performed for both compounds (**4g** and **4m**). The results are shown in Figure 4.

For both complexes, the stability of the systems was preserved, as shown in Figure 4A,B,F,G. The primer influential residue for the stabilization was determined as Glu1088. However, compounds **4g** and **4m** displayed different localizations, similar to docking studies, and thus their interacted parts with Glu1088 differed, as shown in Figure 4C–E,H–J. The hydrazone moiety of compound **4g** directly interacted with Glu1088, while both the hydrazone moiety and thiazole nitrogen of compound **4m** interacted *via* metal-chelating with the same residue. The bond strength of compound **4m** was greater than that of **4g**'s. On the other hand, compound **4m** also interacted with Arg1122 *via* water-mediated H-bond even if it was just a pinch, but it did not show sufficient affinity to Arg458 or other amino acids as found in the docking study; hence, it suggests that its inhibition activity was rooted in metal-chelating. On the contrary, compound **4g** formed two water-mediated H-bonds with Arg458 and Ala1120, yet all of its interactions were not found to be stable at the end of the simulation. Besides that, since the interactions with DNA nucleotides are not generated as the plot by the program, those interactions can be viewed in Video 1_4g and Video 1_4m. As seen, both compounds have interacted with DT:8, DG:9, DC:12, and DA:13 nucleotides *via* π–π stackings. Especially, compound **4g** stacked to DG:9 nucleotide; therefore, we suggest that its activity was based on this connection. So, as a result, those compounds were in good relationship with the DNA; hence, it was concluded that they poisoned the DNA nucleotides to show their function in the same way as fluoroquinolone drugs.

2.6.3. Binding Modes on Lanosterol 14α-Demethylase Enzyme and SAR. The best docking poses and their interaction indices are shared in Figure 5 and Table 9.

Tyr118 residue and HEM protein, according to the literature,[51] play critical roles in inhibition activity. Additionally, Tyr132, Gly303, and Ser378 amino acids are defined as ligand-contacting residues and they have an additional role for different fungal species. Moreover, Met508 is identified as a substrate-binding region like Tyr118 and Tyr132, but it is not responsible for supporting HEM protein. That is why it is suggested that among the other active pocket amino residues, Tyr118 and HEM are essential for the activity, but alone their interaction with β4 hairpin amino acids (like Ser507 and Met508) is not sufficient to inhibit the enzyme activity. However, the interaction with the β4 hairpin region may increase the activity.[52]

In this study, the results revealed that the active compounds against CYP51A have two common interactions. One was found between the thiazole ring and Tyr118 amino acid, and the other was found between the quinoline ring and HEM601, both of which were π–π stackings. Additionally, the hydrazone moiety of the active compounds formed one H-bond with Tyr132 residue, except **4b**; nonetheless, compound **4b** has two aromatic H-bonds in addition to two common interactions with Gly303 and Ser378 amino acids. As mentioned above, all interactions support the results of antifungal tests and enzyme activities.

Besides, compounds **4e**, **4i**, and **4k** could not sit in the active pocket due to their substitutions. Therefore, their action mechanism should go on another pathway. All three have the capability to form a H-bond. Also, docking results point out that they were under solvent exposure; in other words, maybe some of their physicochemical properties such as TPSA and lipophilicity are not proper to the CYP51A enzyme.
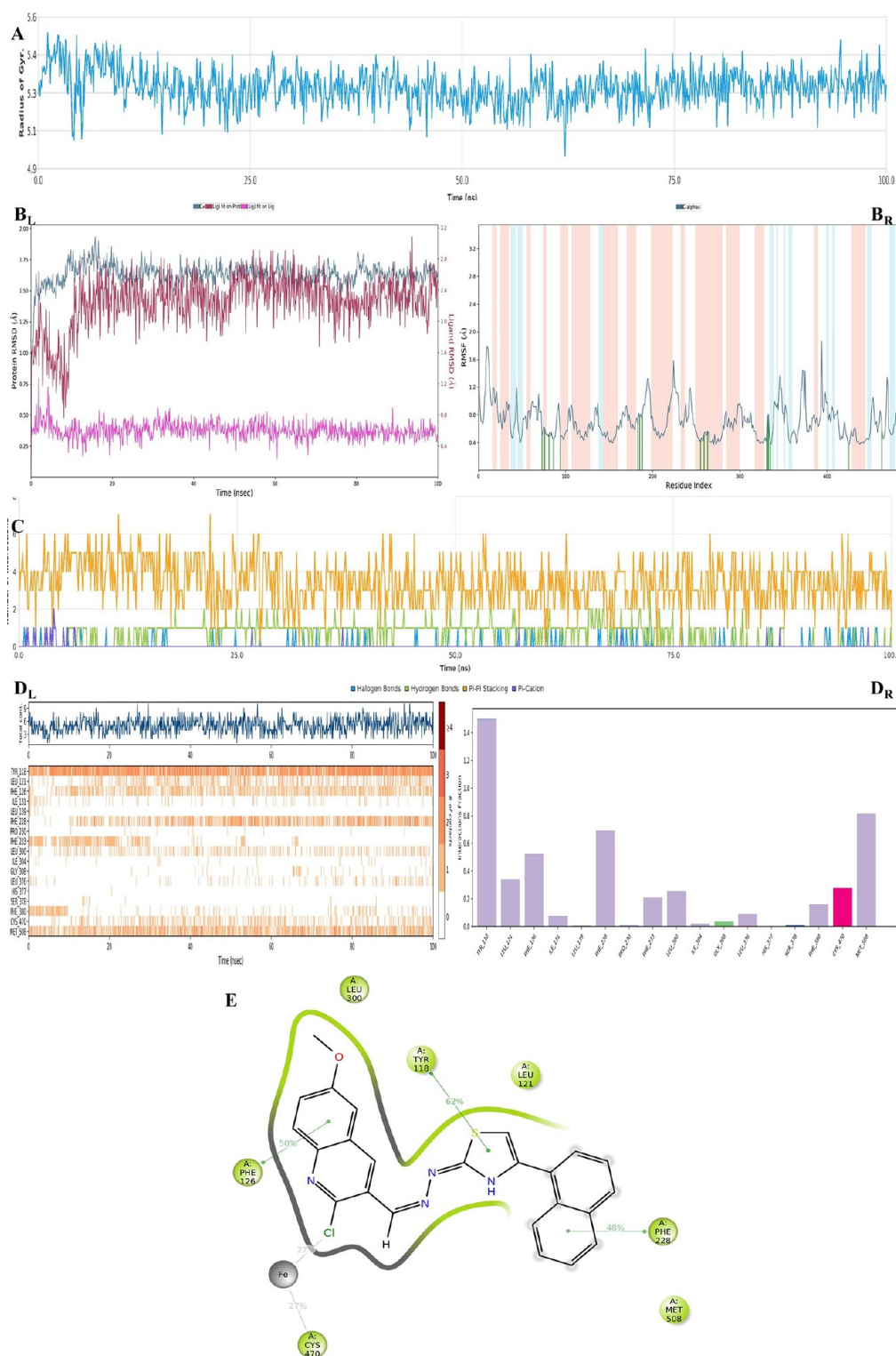
Figure 6. Plots of the MDS results for compound **4m**−LDM enzyme complex. The stability properties (R_g, RMSD, and RMSF plots, respectively) are in (A) and (B) sections. The interaction properties ((C) number of interactions−interaction types−time plot; (D_R) interaction fraction−residue diagram; (D_L) total connections−residues−time plot; and (E) 2D interaction pose with connection strength (cutoff = 0.2) at the active region) are in (C)−(E) sections.

In conclusion, the hybridization of the quinoline, hydrazone, and 4-arylthiazole moieties is significantly effective on this enzyme, which explains how they interacted. Also, 2-chloro-6-methoxyquinolin ring was marked as a pharmacophore group since it contacted the HEM protein.

For further understanding of the SAR, MDS analysis was performed using the best pose of the **4m**−LDS enzyme complex, and this complex was used as a pattern for other active analogues. The results are shown in Figure 6.
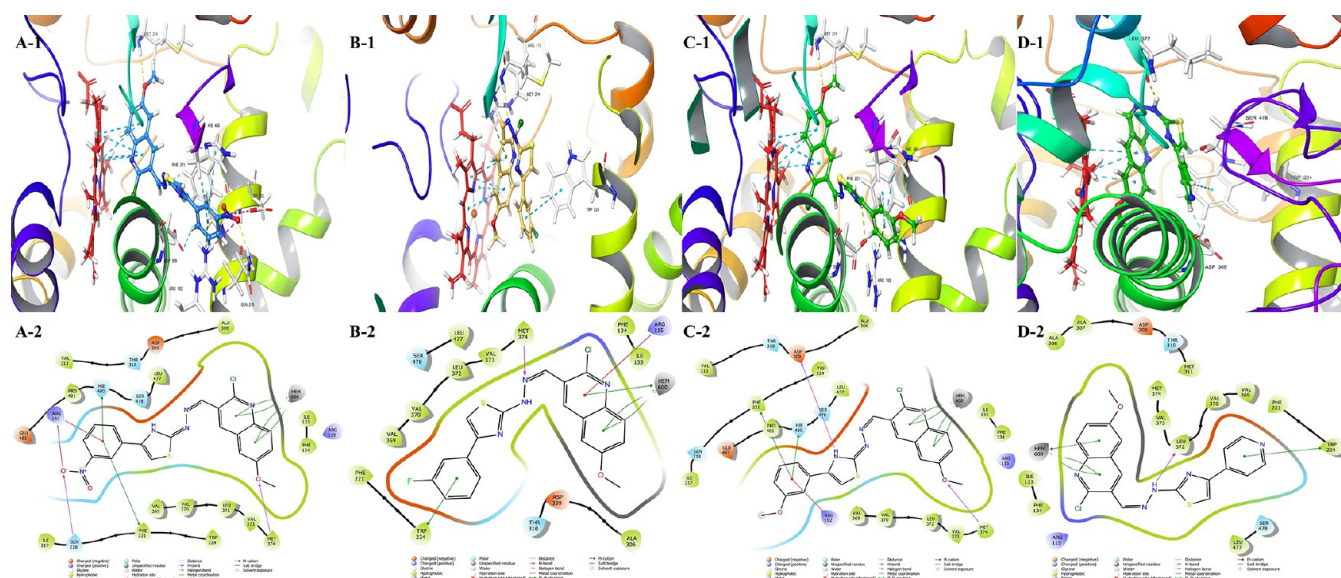
Figure 7. Docking poses of the active compounds in the active side of the aromatase enzyme (PDB ID: 3EQM). 2D and 3D poses of the compounds were viewed. (A) Compound **4i**, (B) compound **4j**, (C) compound **4k**, and (D) compound **4l**.

Table 10. Interaction Index for the Active Compounds—Aromatase Enzyme Complex

compound	ligand moiety	residue	interaction type, count
4i	NO$_2$ group of the phenyl ring	Ar192	1 salt bridge
	phenyl ring	Arg192	1 π−cation interaction
	NO$_2$ group of the phenyl ring	Gln218	1 H-bond
	phenyl ring	Phe221	1 π−π stacking
	N$_1$H of hydrazone	Phe221	1 Ar H-bond
	NO$_2$ group of the phenyl ring	Asp222	1 salt bridge
	C$_5$H of the phenyl ring	Asp309	1 Ar H-bond
	methoxy group of the quinoline ring	Met374	1 H-bond
	phenyl ring	His480	1 π−π stacking
	NO$_2$ group of the phenyl ring	His480	1 Ar H-bond
	quinoline ring	HEM600	5 π−π stackings
4j	quinoline ring	Ar115	1 π−cation interaction
	phenyl ring	Trp224	1 π−π stacking
	N$_1$ of hydrazone	Met374	1 H-bond
	quinoline ring	HEM600	4 π−π stackings
4k	phenyl ring	Arg192	1 π−cation interaction
	phenyl ring	Phe221	1 π−π stacking
	NH of the thiazole ring	Asp309	1 H-bond
	C$_5$H of the phenyl ring	Asp309	1 Ar H-bond
	methoxy group of the quinoline ring	Met374	1 H-bond
	phenyl ring	His480	1 π−π stacking
	NO$_2$ group of the phenyl ring	His480	1 Ar H-bond
	quinoline ring	HEM600	4 π−π stackings
4l	pyridine ring	Trp224	1 π−π stacking
	C$_5$H of the pyridine ring	Asp309	1 Ar H-bond
	N$_1$H of hydrazone	Leu372	1 H-bond
	C$_2$H of the pyridine ring	Ser478	1 Ar H-bond
	quinoline ring	HEM600	3 π−π stackings

As seen in Figure 6A,B, the complex was stable during the entire simulation. The firm interactions were observed between the ligand and Tyr118 (helix B′), Phe228 (helix F″), and

Met508 (β4 hairpin) residues. Chelating with the iron of the HEME protein starts approximately 10 ns after the interaction with Phe228 amino acid, and at the same time, the interaction with Phe380 is over. The RMSD plot and Video 2 clearly show that compound **4m** has undergone a conformational change. As with the molecular docking result, the interactions between Tyr118 and HEM protein (and also its iron) were confirmed by the MDS study for the importance of its inhibition activity. Aromatic substitution (in this case, a 4-naphthalenylthiazole ring was used to exemplify their analogues) interacted with Phe228. This residue is a part of the substrate access channel,[52] and our study showed that this access point was blocked by the naphthalene moiety of the ligand. Therefore, we foresee that the bulky, aromatic groups may increase inhibition activity *via* occluding the access channel. Although our docking results did not show this interaction with any active compounds, this interaction was confirmed in MDS results for compound **4m**. It will probably result in similar interaction between the phenyl ring and Phe228 for the other active compounds.

In conclusion, the 2-chloro-6-methoxyquinoline ring and its thiazole derivatives whose structural importance was explained in *in silico* studies have great potential against the LMD enzyme. For further studies, these moieties will be reconsidered and optimized according to the above information.

2.6.4. Aromatase Enzyme Binding Modes and SAR. The best docking poses and their interaction indices are shared in Figure 7 and Table 10.
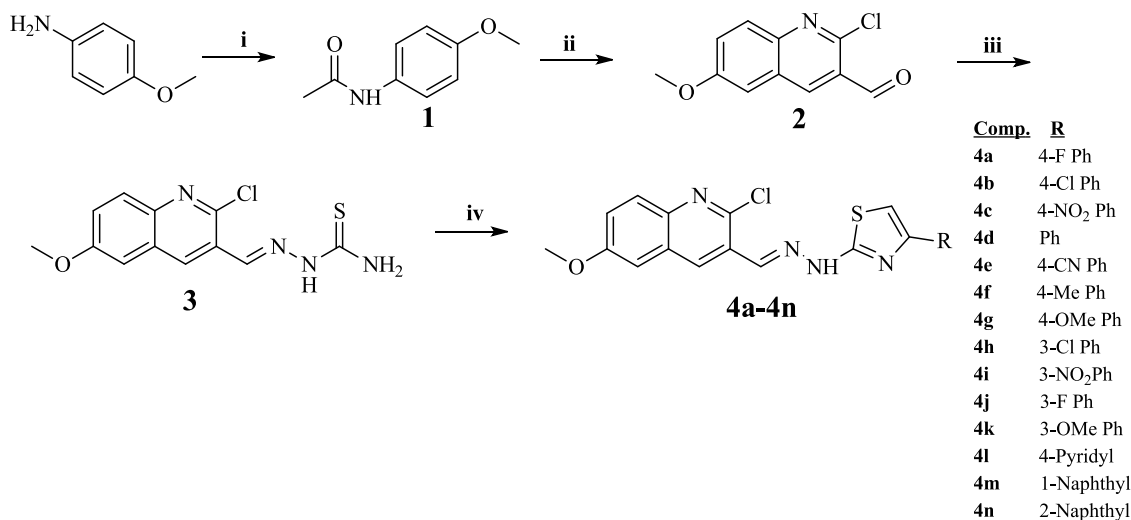
According to the works of the literature,[53,54] the substrate is held above the HEME protein by the 3′-flanking loop region (Pro368−Met374), the I helix (between Glu302 and Thr310), the B′−C loop (containing Ile133 and Phe134), and the four sheets (containing Ser478 and His480). Therefore, in addition to interactions with the HEM protein, interactions with these amino acids are also important to show the ligands' inhibition activity. Also, Met374, Asp309, and Thr310 amino acids were identified as the most important residues in the active regions. Our docking study showed that all active compounds (**4i−l**) interacted with HEM600 (π−π stackings). Compounds **4j** and **4l** have also interacted with Trp224 as common residues. Besides, only compound **4j** interacted with Arg115, and only

Figure 8. Plots of the MDS results for compound **4i**−aromatase enzyme complex. The stability properties (R_g, RMSD, and RMSF plots, respectively) are in (A) and (B) sections. The interaction properties ((C) number of interactions−interaction types−time plot; (D_R) interaction fraction−residue diagram; (D_L) total connections−residues−time plot; and (E) 2D interaction pose with connection strength (cutoff = 0.2) at the active region) are in (C)−(E) sections.

compound **4l** formed a H-bond with Leu372. Moreover, only compound **4l** did not form a H-bond with Met374 amino acid, but instead of that, compound **4l** interacted with Leu372, which is a member of the same β-strand region. The most active compounds **4i** and **4k** were fit at the aromatase enzyme active

region very similarly. Both interacted with Ar192, Phe221, Asp309, Met374, His480, and HEM600. The differences between them are the interaction numbers of the above residues and interactions with Gln218 and Asp222. Only compound **4i** forms H-bonds with these residues, so its inhibitory effect may

Scheme 1. General Procedure for the Synthesis of the Compounds[a]

Comp.	R
4a	4-F Ph
4b	4-Cl Ph
4c	4-NO₂ Ph
4d	Ph
4e	4-CN Ph
4f	4-Me Ph
4g	4-OMe Ph
4h	3-Cl Ph
4i	3-NO₂Ph
4j	3-F Ph
4k	3-OMe Ph
4l	4-Pyridyl
4m	1-Naphthyl
4n	2-Naphthyl

[a]Reactions and conditions: (i) CH₃COCl, tetrahydrofuran (THF), TEA, 0 °C, after dropping, room temperature (rt), 4 h; (ii) Vilsmeier−Haack reagent, 0 °C, then water bath, 8 h; (iii) thiosemicarbazide, EtOH, rt, 2 h; and (iv) 2-bromoethanone derivatives, EtOH, rt, 2 h.

be increased because of that. As a result, *in vitro* results are supported by the docking results, and the *in silico* study gave a first sight of the structure−activity relationship at the molecular level.

For further understanding of the SAR, MDS analysis was performed using the best pose of the **4i**−aromatase enzyme complex, and this complex was used as a pattern for other active analogues. The results are shown in Figure 8.

Figure 8A,B points out that the stability of the complex was protected during the simulation. According to the inhibition mechanism of the aromatase enzyme, the effect of ligands has been related to either stabilization of the loop amino acids or stabilization of other regional amino acids on the active site of the enzyme that interacted with loop amino acids. Therefore, stability is mainly related to the stabilization of the loop regions. In this case (see Figure 8C−E and Video 3), it can be suggested that Arg309 (I helices), Met374 (3′-flanking loop), and His480 (β4 sheet) residues have a pivotal role considering their bond strength and their interaction continuity. Therefore, enzyme substrates cannot achieve the active region for aromatization to be ergosterol. Furthermore, the chlorine of compound **4i**'s quinoline ring chelated with the iron of the HEM protein, which is critical for the inhibition activity of the aromatase enzyme. In conclusion, the 2-chloro-6-methoxyquinoline ring was declared as the pharmacophore structure for aromatase inhibition, and its mechanism was explained.

3. SAR SUMMARY

The compounds were designed and synthesized for a good antimicrobial activity profile with fewer side effects. Even though the primary aim was to find antibacterial activity with less toxicity against healthy cells, we found that their antifungal activity was more distinctive. Thus, our study was shaped by the antifungal activity after this step. For this, the active compounds were tested for their inhibition effect against LDM, and the possible side effects of the compounds were determined *via* testing the active compounds against the aromatase enzyme in addition to their cytotoxicity profile on healthy cells. After elimination by various tests, only compounds **4b**, **4f**, **4h**, and **4m** have passed the tests as antifungal agents. We suggest that these

compounds can be used as antifungal agents after the completion of all testing studies. Moreover, mechanistic studies showed that the core structure of 2-chloro-6-methoxyquinoline and thiazole hybridization has great antifungal potential with fewer side effect profiles unless the substitutions are not in the third position on the phenyl ring or heteroaromatics. The bulky groups (such as 1-naphthalene) also affected the activity positively. On the other hand, all of these unfavorable groups increased the inhibitory activity of the aromatase enzyme. Thus, mentioned as unfavorable, third substitutions can be used in special cases who are suffering from fungal infections in addition to primer diseases such as cancer and transplant patients, but it is not the aim of this study. Hence, those purposes should be evaluated for further study.

4. CONCLUSIONS

A new series of quinoline derivatives were designed, synthesized, and analyzed. The final molecules were evaluated for their antimicrobial properties and then clarified their action mechanisms using various *in vitro* and *in silico* methods. Their antimicrobial activity was tested against six bacteria and four *Candida* species. Their cytotoxicity effects were determined against NIH/3T3 cell lines, and their action mechanisms were investigated on DNA gyrase, LDM, and aromatase enzyme. All of these results were inspected at the molecular level by docking and dynamic simulation studies and clarified their action mechanisms. Compounds **4b**, **4f**, **4h**, and **4m** have a good antifungal profile with low side effects, while compounds **4j** and **4l** can be used alone for special patients suffering from fungal infection in addition to primer disease considering their possible side effects. At least the drug interactions can be minimalized for these patients. Generally, it was announced that compound **4m** has potential antimicrobial, especially, anticandidal activity, with a trustable therapeutic index and potentially fewer side effects.

5. EXPERIMENTAL SECTION

5.1. Chemistry. All chemicals were purchased from Sigma-Aldrich Chemical Co. (Sigma-Aldrich Corp., St. Louis, MO) and Merck Chemicals (Merck KGaA, Darmstadt, Germany). All melting points (m.p.) were determined by an MP90 digital

melting point apparatus (Mettler Toledo, Ohio) and were uncorrected. All reactions were monitored by thin-layer chromatography (TLC) using Silica Gel 60 F254 TLC plates (Merck KGaA, Darmstadt, Germany). Spectroscopic data were recorded with the following instruments: ^{1}H nuclear magnetic resonance (NMR) Bruker DPX-300 FT NMR spectrometer, ^{13}C NMR, Bruker DPX 75 MHz spectrometer (Bruker Bioscience, Billerica, MA); mass (high-resolution mass spectrometry (HRMS)) spectra were recorded on a liquid chromatography connected with hybrid ion-trap and time-of-flight mass spectrometry (Shimadzu) using electrospray ionization.

5.1.1. Synthesis of 4′-Methoxyacetanilide (1). 4-Anisidine (0.065 mol) and triethylamine (TEA) (0.078 mol) were dissolved in dichloromethane in a flask and placed in an ice bath at 0−5 °C. On the other hand, acetyl chloride (0.09 mol) was dissolved in dichloromethane in the dropping funnel and dropped carefully into the mixture in the flask. In the meantime, care was taken to mix the mixture vigorously. After the dripping was finished, it was left to stir for another 3 h at room temperature. The end of the reaction was checked with TLC. The solvent was completely evaporated, and the solid was washed with water, filtered, and then dried. The product was crystallized from ethanol.

5.1.2. Synthesis of 2-Chloro-6-methoxyquinoline-3-carbaldehyde (2). N-(4-Methoxyphenyl)acetamide (**1**, 1 equiv) was stirred with Vilsmeier reagent in a hot water bath. After 4 h of stirring, the reaction was checked with TLC. Then, the mixture in the balloon was poured into the icy water. The solid product was washed with water, filtered, and left to dry. The dried product was crystallized from ethanol.

5.1.3. Synthesis of 2-[(2-Chloro-6-methoxyquinolin-3-yl)-methylene]hydrazine-1-carbothioamide (3). 2-Chloro-6-methoxyquinoline-3-carbaldehyde (**2**, 0.040 mol) and thiosemicarbazide (0.040 mol) were refluxed in ethanol. The reaction was terminated by TLC control. The precipitated part was filtered and separated from the alcohol. After the solvent was evaporated, the crude product was crystallized from ethanol.

5.1.4. 2-[2-((2-Chloro-6-methoxyquinolin-3-yl)-methylene)hydrazinyl]-4-Substituted Thiazole Derivatives (4a−m). 1-Aryl-2-bromoethanone derivatives taken in equal moles with 2-[(2-chloro-6-methoxyquinolin-3-yl)methylene]-hydrazine-1-carbothioamide were refluxed in alcohol for 2 h. The end of the reaction was controlled with TLC, and the final products were filtered and separated from the alcohol. After the solvent was evaporated, the crude products were recrystallized from ethanol.

The reaction procedure is displayed in Scheme 1. The synthesized compounds and their results of the spectra are shared between Sections 1.1 and 1.14 in the Supporting Information.

5.2. Antimicrobial Activity Studies. *E. coli* (ATCC 35218), *E. coli* (ATCC 25922), *S. aureus* (ATCC 6538), methicillin-resistant *S. aureus* (MRSA) (clinical isolate), *S. typhimurium* (ATCC 13311), and *K. pneumoniae* (NCTC 9633) cells for antibacterial effect, and *C. albicans* (ATCC 24433), *C. glabrata* (ATCC 90030), *C. krusei* (ATCC 6258), and *C. parapsilosis* (ATCC 22019) for the antifungal effect of the final compounds were used to determine the MIC$_{90}$ values. The broth microdilution procedure specified in the M07-A9 document of the Clinical and Laboratory Standards Institute (CLSI) was used for antibacterial study,[55] and the EDef 7.1 document published by EUCAST was used for the antifungal

study.[56] For both activity studies, the detailed procedures were explained in previous studies.[57,58]

5.3. Cytotoxic Evaluation of the Final Compounds. NIH/3T3 cells were incubated in Dulbecco's modified Eagle's medium (DMEM) (Sigma-Aldrich, St. Louis, MO), added with fetal calf serum, penicillin (100 IU/mL), streptomycin (100 mg/mL), and 7.5% NaHCO$_3$ at 37 °C in a humidified atmosphere of 95% air and 5% CO$_2$. NIH/3T3 cells were seeded into the 96-well plates at a density of 1×10^4 cells. After 24 h of incubating period, the culture media were removed, and test compounds were added. After 24 h of incubation period, colorimetric measurements were performed by a microplate reader (Biotek) at 540 nm. Inhibition % at all concentrations was determined using the formula below, and the IC$_{50}$ values were calculated from a dose−response curve obtained by plotting the percentage inhibition *versus* the log concentration with the use of Microsoft Excel 2013. The results were displayed as mean ± standard deviation (SD).[59−61]

5.4. Enzyme Inhibition Tests. *5.4.1. Inhibition of DNA-Gyrase Enzyme.* DNA gyrase obtained from *E. coli* was used to detect the inhibition of the superhelix activity of DNA gyrase. The method was performed according to the kit protocol described by the supplier (SKU TG2000G-3, TopoGen). The detailed procedures were explained in the previous study.[62]

5.4.2. Inhibition of Fungal LDM Enzyme. Ergosterol level was determined using the extract of total sterols from *C. albicans* (and its other species) following the method described by Breivik and Owades.[63] Quantification of the ergosterol level in this extract was carried out by the recently described method.[58,64−66] According to these described studies, in the current work, compounds **4b**, **4e**, **4f**, and **4h−m** were undertaken to investigate their action mechanism. Thus, the LC-MS-MS-based method that quantifies the ergosterol level was applied. All active anticandidal compounds, ketoconazole, and fluconazole were used at 3.91, 0.98, 0.24, and 0.06 μg/mL concentrations. Ergosterol quantity in negative control samples was regarded as 100%. All concentrations were analyzed in quadruplicate, and the results were expressed as mean ± standard deviation (SD).

5.4.3. Inhibition of Human Aromatase Enzyme. Since targeting human aromatase enzyme was reported for antifungal activity and it plays a pivotal role in fungal cell function,[40] compounds that showed antifungal activity were evaluated for inhibition activity on aromatase enzyme using a kit procedure (Bio Vision, Aromatase (CYP19A) Inhibitor Screening Kit (Fluorometric)), as described in previous studies.[67−69]

5.5. *In Silico* Studies. The pharmacokinetic profile was predicted *via in silico* methods. The active compounds may be considered in the future for *in vivo* pharmacokinetic studies as the current study is involved basically in the evaluation of the activity. Therefore, the medicinal chemistry and pharmacokinetic profiles of the designed compounds were calculated using the Swiss-ADME web-based program.[70]

All docking studies on various enzymes were performed using the Schrodinger Maestro Suite program. The interfaces of this program are used for the protein preparation process, ligand preparation process, grid generation, docking, and visualization studies.[71−73] The crystal structure of the enzymes was retrieved from the Protein Data Bank server (PDB codes: 2XCT, 3EQM, and 5TZ1 for DNA gyrase, aromatase, and lanosterol 14α-demethylase). All ligands were set to the physiological pH (pH = 7.4) at the protonation step. The proteins were prepared according to the previous studies.[34,62,67]

The molecular dynamics simulations (MDS) were performed using the Maestro Desmond interface program.[74] All molecular dynamics simulations (MDS) for 100 ns were carried out to analyze the stability of the identified hits from the *in vitro* docking results. Preparing the system setup, performing molecular dynamics simulations, and calculating the interaction analysis were carried out according to the same procedure as previous studies.[67,75] All systems were set up using "System Builder" in Maestro. The complex structure was subjected to energy minimization (OPLS3e standard force field). Transferable intermolecular potential with the 3-point water model was used for the creation of the hydration model. The neutralization of the system was achieved using Na^+ and Cl^- ions. The molecular dynamic simulation was performed following the completion of the system setup. The radius of gyration (R_g), root-mean-square fluctuation (RMSF), and root-mean-square deviation (RMSD) values were calculated by the Desmond application.

ASSOCIATED CONTENT

Supporting Information

The Supporting Information is available free of charge at https://pubs.acs.org/doi/10.1021/acsomega.2c06871.

> Analytical spectra (HRMS, ^1H NMR, and ^{13}C NMR), analytical results, and InChI descriptions of the synthesized compounds (PDF)

> DNA-gyrase—DNA complex (Video 1_**4g**) (AVI)

> DNA-gyrase—DNA complex (Video 1_**4m**) (AVI)

> LDM complex (Video 2) (AVI)

> Aromatase complex (Video 3) (AVI)

AUTHOR INFORMATION

Corresponding Authors

Asaf Evrim Evren — *Department of Pharmacy Services, Vocational School of Health Services, Bilecik Şeyh Edebali University, Bilecik 11000, Turkey; Department of Pharmaceutical Chemistry, Faculty of Pharmacy, Anadolu University, Eskişehir 26470, Turkey;* orcid.org/0000-0002-8651-826X; Email: asafevrimevren@anadolu.edu.tr, asafevrim.evren@bilecik.edu.tr

Leyla Yurttaş — *Department of Pharmaceutical Chemistry, Faculty of Pharmacy, Anadolu University, Eskişehir 26470, Turkey;* Email: lyurttas@anadolu.edu.tr

Authors

Abdullah Burak Karaduman — *Department of Pharmaceutical Toxicology, Faculty of Pharmacy, Anadolu University, Eskişehir 26470, Turkey*

Begüm Nurpelin Sağlik — *Department of Pharmaceutical Chemistry, Faculty of Pharmacy, Anadolu University, Eskişehir 26470, Turkey; Central Research Laboratory, Faculty of Pharmacy, Anadolu University, Eskişehir 26470, Turkey;* orcid.org/0000-0002-0151-6266

Yusuf Özkay — *Department of Pharmaceutical Chemistry, Faculty of Pharmacy, Anadolu University, Eskişehir 26470, Turkey; Central Research Laboratory, Faculty of Pharmacy, Anadolu University, Eskişehir 26470, Turkey*

Complete contact information is available at:
https://pubs.acs.org/10.1021/acsomega.2c06871

Author Contributions

Conceptualization and validation, L.Y., A.E.E., and Y.O.; methodology, software, and formal analysis, A.E.E. and B.N.S.; investigation, A.E.E., B.N.S., and A.B.K.; resources, L.Y., A.E.E. and B.N.S.; data curation and writing—original draft preparation, L.Y. and A.E.E.; writing—review and editing, B.N.S., A.B.K., and Y.O.; visualization, A.E.E. and B.N.S.; and supervision, L.Y. and Y.O.

Notes

The authors declare no competing financial interest.

REFERENCES

(1) Schlossberg, D. *Clinical Infectious Disease*; Cambridge University Press: Philadelphia, 2015.

(2) Alberts, B.; Johnson, A.; Lewis, J.; Walter, P.; Raff, M.; Roberts, K. *Pathogens, Infection, and Innate Immunity*, International Student ed.; Routledge: New York, 2002; pp 1485−1538.

(3) Peng, X. M.; Cai, G. X.; Zhou, C. H. Recent developments in azole compounds as antibacterial and antifungal agents. *Curr. Top. Med. Chem.* **2013**, *13*, 1963−2010.

(4) Ramirez-Garcia, A.; Rementeria, A.; Aguirre-Urizar, J. M.; Moragues, M. D.; Antoran, A.; Pellon, A.; Abad-Diaz-de-Cerio, A.; Hernando, F. L. *Candida albicans* and cancer: Can this yeast induce cancer development or progression? *Crit. Rev. Microbiol.* **2016**, *42*, 181−193.

(5) Zasloff, M. Antimicrobial peptides of multicellular organisms. *Nature* **2002**, *415*, 389−395.

(6) Arvanitis, M.; Mylonakis, E. Fungal-bacterial interactions and their relevance in health. *Cell Microbiol.* **2015**, *17*, 1442−1446.

(7) Arsenault, A. B.; Bliss, J. M. Neonatal Candidiasis: New Insights into an Old Problem at a Unique Host-Pathogen Interface. *Curr. Fungal Infect. Rep.* **2015**, *9*, 246−252.

(8) Mead, P. S.; Slutsker, L.; Dietz, V.; McCaig, L. F.; Bresee, J. S.; Shapiro, C.; Griffin, P. M.; Tauxe, R. V. Food-related illness and death in the United States. *Emerging Infect. Dis.* **1999**, *5*, 607−625.

(9) Singh, N.; Rogers, P.; Atwood, C. W.; Wagener, M. M.; Yu, V. L. Short-course empiric antibiotic therapy for patients with pulmonary infiltrates in the intensive care unit. A proposed solution for indiscriminate antibiotic prescription. *Am. J. Respir. Crit. Care Med.* **2000**, *162*, 505−511.

(10) Zehra, A.; Gulzar, M.; Singh, R.; Kaur, S.; Gill, J. P. S. Prevalence, multidrug resistance and molecular typing of methicillin-resistant *Staphylococcus aureus* (MRSA) in retail meat from Punjab, India. *J. Global Antimicrob. Resist.* **2019**, *16*, 152−158.

(11) Tfifha, M.; Ferjani, A.; Mallouli, M.; Mlika, N.; Abroug, S.; Boukadida, J. Carriage of multidrug-resistant bacteria among pediatric patients before and during their hospitalization in a tertiary pediatric unit in Tunisia. *Libyan J. Med.* **2018**, *13*, No. 1419047.

(12) Miyanaga, M.; Nejima, R.; Miyai, T.; Miyata, K.; Ohashi, Y.; Inoue, Y.; Toyokawa, M.; Asari, S. Changes in drug susceptibility and the quinolone-resistance determining region of *Staphylococcus epidermidis* after administration of fluoroquinolones. *J. Cataract Refractive Surg.* **2009**, *35*, 1970−1978.

(13) Todd, B. Reconsidering Antibiotic Resistance. *Am. J. Nurs.* **2017**, *117*, 66−67.

(14) Spellberg, B. The New Antibiotic Mantra-″Shorter Is Better″. *JAMA Intern. Med.* **2016**, *176*, 1254−1255.

(15) Khan, Z.; Ahmad, S.; Benwan, K.; Purohit, P.; Al-Obaid, I.; Bafna, R.; Emara, M.; Mokaddas, E.; Abdullah, A. A.; Al-Obaid, K.; Joseph, L. Invasive Candida auris infections in Kuwait hospitals: epidemiology, antifungal treatment and outcome. *Infection* **2018**, *46*, 641−650.

(16) Nweke, M. C.; Okolo, C. A.; Daous, Y.; Esan, O. A. Challenges of Human Papillomavirus Infection and Associated Diseases in Low-Resource Countries. *Arch. Pathol. Lab. Med.* **2018**, *142*, 696−699.

(17) Levy, S. B.; Marshall, B. Antibacterial resistance worldwide: causes, challenges and responses. *Nat. Med.* **2004**, *10*, S122−S129.

(18) Buchanan, P.; Courtenay, M. Treatment of Infection. *Prescribing in Dermatology*; Cambridge University Press: Philadelphia, 2006; pp 20−25.

(19) Ronald, A. R.; Turck, M.; Petersdorf, R. G. A critical evaluation of nalidixic acid in urinary-tract infections. *N. Engl. J. Med.* **1966**, *275*, 1081−1089.

(20) Hu, G.; Wang, G.; Duan, N.; Wen, X.; Cao, T.; Xie, S.; Huang, W. Design, synthesis and antitumor activities of fluoroquinolone C-3 heterocycles (IV): s-triazole Schiff−Mannich bases derived from ofloxacin. *Acta Pharm. Sin. B* **2012**, *2*, 312−317.

(21) Saura, C.; Garcia-Saenz, J. A.; Xu, B.; Harb, W.; Moroose, R.; Pluard, T.; Cortes, J.; Kiger, C.; Germa, C.; Wang, K.; Martin, M.; Baselga, J.; Kim, S. B. Safety and efficacy of neratinib in combination with capecitabine in patients with metastatic human epidermal growth factor receptor 2-positive breast cancer. *J. Clin. Oncol.* **2014**, *32*, 3626−3633.

(22) Li, N.; Song, Y.; Du, P.; Shen, Y.; Yang, J.; Gui, L.; Wang, S.; Wang, J.; Sun, Y.; Han, X.; Shi, Y. Oral topotecan: Bioavailability, pharmacokinetics and impact of ABCG2 genotyping in Chinese patients with advanced cancers. *Biomed. Pharmacother.* **2013**, *67*, 801−806.

(23) Watt, P. M.; Hickson, I. D. Structure and function of type II DNA topoisomerases. *Biochem. J.* **1994**, *303*, 681−695.

(24) Musiol, R.; Serda, M.; Hensel-Bielowka, S.; Polanski, J. Quinoline-based antifungals. *Curr. Med. Chem.* **2010**, *17*, 1960−1973.

(25) Senerovic, L.; Opsenica, D.; Moric, I.; Aleksic, I.; Spasic, M.; Vasiljevic, B.Quinolines and Quinolones as Antibacterial, Antifungal, Anti-virulence, Antiviral and Anti-parasitic Agents. In *Advances in Experimental Medicine and Biology*; Springer, 2020; Vol. *1282*, pp 37−69.

(26) Chen, Y. J.; Ma, K. Y.; Du, S. S.; Zhang, Z. J.; Wu, T. L.; Sun, Y.; Liu, Y. Q.; Yin, X. D.; Zhou, R.; Yan, Y. F.; Wang, R. X.; He, Y. H.; Chu, Q. R.; Tang, C. Antifungal Exploration of Quinoline Derivatives against Phytopathogenic Fungi Inspired by Quinine Alkaloids. *J. Agric. Food Chem.* **2021**, *69*, 12156−12170.

(27) Dhingra, S.; Cramer, R. A. Regulation of Sterol Biosynthesis in the Human Fungal Pathogen *Aspergillus fumigatus*: Opportunities for Therapeutic Development. *Front. Microbiol.* **2017**, *8*, No. 92.

(28) Lupetti, A.; Danesi, R.; Campa, M.; Del Tacca, M.; Kelly, S. Molecular basis of resistance to azole antifungals. *Trends Mol. Med.* **2002**, *8*, 76−81.

(29) Verma, A. K.; Majid, A.; Hossain, M. S.; Ahmed, S. F.; Ashid, M.; Bhojiya, A. A.; Upadhyay, S. K.; Vishvakarma, N. K.; Alam, M. Identification of 1, 2, 4-Triazine and Its Derivatives Against Lanosterol 14-Demethylase (CYP51) Property of *Candida albicans*: Influence on the Development of New Antifungal Therapeutic Strategies. *Front. Med. Technol.* **2022**, *4*, No. 845322.

(30) Zhang, W.; Ramamoorthy, Y.; Kilicarslan, T.; Nolte, H.; Tyndale, R. F.; Sellers, E. M. Inhibition of cytochromes P450 by antifungal imidazole derivatives. *Drug Metab. Dispos.* **2002**, *30*, 314−318.

(31) Sheng, C.; Miao, Z.; Ji, H.; Yao, J.; Wang, W.; Che, X.; Dong, G.; Lu, J.; Guo, W.; Zhang, W. Three-dimensional model of lanosterol 14 alpha-demethylase from Cryptococcus neoformans: active-site characterization and insights into azole binding. *Antimicrob. Agents Chemother.* **2009**, *53*, 3487−3495.

(32) Guedes, P. M. d. M.; Urbina, J. A.; de Lana, M.; Afonso, L. C.; Veloso, V. M.; Tafuri, W. L.; Machado-Coelho, G. L.; Chiari, E.; Bahia, M. T. Activity of the new triazole derivative albaconazole against *Trypanosoma (Schizotrypanum) cruzi* in dog hosts. *Antimicrob. Agents Chemother.* **2004**, *48*, 4286−4292.

(33) Yadav, M.; Lal, K.; Kumar, A.; Kumar, A.; Kumar, D. Indole-chalcone linked 1,2,3-triazole hybrids: Facile synthesis, antimicrobial evaluation and docking studies as potential antimicrobial agents. *J. Mol. Struct.* **2022**, *1261*, No. 132867.

(34) Lebouvier, N.; Pagniez, F.; Na, Y. M.; Shi, D.; Pinson, P.; Marchivie, M.; Guillon, J.; Hakki, T.; Bernhardt, R.; Yee, S. W.; Simons, C.; Leze, M. P.; Hartmann, R. W.; Mularoni, A.; Le Baut, G.; Krimm, I.;

Abagyan, R.; Le Pape, P.; Le Borgne, M. Synthesis, Optimization, Antifungal Activity, Selectivity, and CYP51 Binding of New 2-Aryl-3-azolyl-1-indolyl-propan-2-ols. *Pharmaceuticals* **2020**, *13*, No. 186.

(35) Zhu, T.; Chen, X.; Li, C.; Tu, J.; Liu, N.; Xu, D.; Sheng, C. Lanosterol 14alpha-demethylase (CYP51)/histone deacetylase (HDAC) dual inhibitors for treatment of *Candida tropicalis* and *Cryptococcus neoformans* infections. *Eur. J. Med. Chem.* **2021**, *221*, No. 113524.

(36) Maccallini, C.; Gallorini, M.; Sisto, F.; Akdemir, A.; Ammazzalorso, A.; De Filippis, B.; Fantacuzzi, M.; Giampietro, L.; Carradori, S.; Cataldi, A.; Amoroso, R. New azolyl-derivatives as multitargeting agents against breast cancer and fungal infections: synthesis, biological evaluation and docking study. *J. Enzyme Inhib. Med. Chem.* **2021**, *36*, 1632−1645.

(37) Friggeri, L.; Hargrove, T. Y.; Wawrzak, Z.; Guengerich, F. P.; Lepesheva, G. I. Validation of Human Sterol 14alpha-Demethylase (CYP51) Druggability: Structure-Guided Design, Synthesis, and Evaluation of Stoichiometric, Functionally Irreversible Inhibitors. *J. Med. Chem.* **2019**, *62*, 10391−10401.

(38) Zarn, J. A.; Bruschweiler, B. J.; Schlatter, J. R. Azole fungicides affect mammalian steroidogenesis by inhibiting sterol 14 alpha-demethylase and aromatase. *Environ. Health Perspect.* **2003**, *111*, 255−261.

(39) Trösken, E. R.; Scholz, K.; Lutz, R. W.; Volkel, W.; Zarn, J. A.; Lutz, W. K. Comparative assessment of the inhibition of recombinant human CYP19 (aromatase) by azoles used in agriculture and as drugs for humans. *Endocr. Res.* **2004**, *30*, 387−394.

(40) Trösken, E. R.; Fischer, K.; Volkel, W.; Lutz, W. K. Inhibition of human CYP19 by azoles used as antifungal agents and aromatase inhibitors, using a new LC-MS/MS method for the analysis of estradiol product formation. *Toxicology* **2006**, *219*, 33−40.

(41) Albengres, E.; Le Louet, H.; Tillement, J. P. Systemic antifungal agents. Drug interactions of clinical significance. *Drug Saf.* **1998**, *18*, 83−97.

(42) Ören, İ.; Temiz, Ö.; Yalçın, İ.; Şener, E.; Altanlar, N. Synthesis and antimicrobial activity of some novel 2,5- and/or 6-substituted benzoxazole and benzimidazole derivatives. *Eur. J. Pharm. Sci.* **1999**, *7*, 153−160.

(43) Erdik, E. *Organik kimyada spektroskopik yöntemler*; Gazi Kitapevi: Ankara, 1998; Vol. *82*.

(44) Erdik, E.; Obalı, M.; Yüksekışık, N.; Öktemer, A.; Pekel, T. *Denel Organik Kimya*, 4th ed.; Gazi Kitabevi: Ankara, Türkiye, 2007.

(45) Li, S.; Luan, G.; Ren, X.; Song, W.; Xu, L.; Xu, M.; Zhu, J.; Dong, D.; Diao, Y.; Liu, X.; Zhu, L.; Wang, R.; Zhao, Z.; Xu, Y.; Li, H. Rational Design of Benzylidenehydrazinyl-Substituted Thiazole Derivatives as Potent Inhibitors of Human Dihydroorotate Dehydrogenase with in Vivo Anti-arthritic Activity. *Sci. Rep.* **2015**, *5*, No. 14836.

(46) Lukeš, V.; Michalík, M.; Poliak, P.; Cagardová, D.; Végh, D.; Bortňák, D.; Fronc, M.; Kožíšek, J. Theoretical and experimental study of model oligothiophenes containing 1-methylene-2-(perfluorophenyl)hydrazine terminal unit. *Synth. Met.* **2016**, *219*, 83−92.

(47) Aly, A. A.; Mohamed, A. H.; Ramadan, M. Synthesis and colon anticancer activity of some novel thiazole/-2-quinolone derivatives. *J. Mol. Struct.* **2020**, *1207*, No. 127798.

(48) Schroeder, G. M.; An, Y.; Cai, Z. W.; Chen, X. T.; Clark, C.; Cornelius, L. A.; Dai, J.; Gullo-Brown, J.; Gupta, A.; Henley, B.; Hunt, J. T.; Jeyaseelan, R.; Kamath, A.; Kim, K.; Lippy, J.; Lombardo, L. J.; Manne, V.; Oppenheimer, S.; Sack, J. S.; Schmidt, R. J.; Shen, G.; Stefanski, K.; Tokarski, J. S.; Trainor, G. L.; Wautlet, B. S.; Wei, D.; Williams, D. K.; Zhang, Y.; Zhang, Y.; Fargnoli, J.; Borzilleri, R. M. Discovery of N-(4-(2-amino-3-chloropyridin-4-yloxy)-3-fluorophen-yl)-4-ethoxy-1-(4-fluorophenyl)-2-oxo-1,2-dihydropyridine-3-carboxa-mide (BMS-777607), a selective and orally efficacious inhibitor of the Met kinase superfamily. *J. Med. Chem.* **2009**, *52*, 1251−1254.

(49) Potts, R. O.; Guy, R. H. Predicting skin permeability. *Pharm. Res.* **1992**, *9*, 663−669.

(50) Chan, P. F.; Srikannathasan, V.; Huang, J.; Cui, H.; Fosberry, A. P.; Gu, M.; Hann, M. M.; Hibbs, M.; Homes, P.; Ingraham, K.; Pizzollo,

J.; Shen, C.; Shillings, A. J.; Spitzfaden, C. E.; Tanner, R.; Theobald, A. J.; Stavenger, R. A.; Bax, B. D.; Gwynn, M. N. Structural basis of DNA gyrase inhibition by antibacterial QPT-1, anticancer drug etoposide and moxifloxacin. *Nat. Commun.* **2015**, *6*, No. 10048.

(51) Hargrove, T. Y.; Friggeri, L.; Wawrzak, Z.; Qi, A.; Hoekstra, W. J.; Schotzinger, R. J.; York, J. D.; Guengerich, F. P.; Lepesheva, G. I. Structural analyses of *Candida albicans* sterol 14alpha-demethylase complexed with azole drugs address the molecular basis of azole-mediated inhibition of fungal sterol biosynthesis. *J. Biol. Chem.* **2017**, *292*, 6728−6743.

(52) Lepesheva, G. I.; Waterman, M. R. Structural basis for conservation in the CYP51 family. *Biochim. Biophys. Acta, Proteins Proteomics* **2011**, *1814*, 88−93.

(53) Park, J.; Czapla, L.; Amaro, R. E. Molecular simulations of aromatase reveal new insights into the mechanism of ligand binding. *J. Chem. Inf. Model.* **2013**, *53*, 2047−2056.

(54) Hong, Y.; Li, H.; Yuan, Y. C.; Chen, S. Molecular characterization of aromatase. *Ann. N. Y. Acad. Sci.* **2009**, *1155*, 112−120.

(55) CLSI. *Methods for Dilution Antimicrobial Susceptibility Tests for Bacteria That Grow Aerobically; Approved Standard*, CLSI document M07-A9, 9th ed.; CLSI, 2012.

(56) Rodriguez-Tudela, J. L.; Arendrup, M.; Barchiesi, F.; et al. EUCAST definitive document EDef 7.1: method for the determination of broth dilution MICs of antifungal agents for fermentative yeasts. *Clin. Microbiol. Infect.* **2008**, *14*, 398−405.

(57) Evren, A. E.; Dawbaa, S.; Nuha, D.; Yavuz, Ş. A.; Gül, Ü. D.; Yurttaş, L. Design and synthesis of new 4-methylthiazole derivatives: In vitro and in silico studies of antimicrobial activity. *J. Mol. Struct.* **2021**, *1241*, No. 130692.

(58) Osmaniye, D.; Kaya Cavusoglu, B.; Saglik, B. N.; Levent, S.; Acar Cevik, U.; Atli, O.; Ozkay, Y.; Kaplancikli, Z. A. Synthesis and Anticandidal Activity of New Imidazole-Chalcones. *Molecules* **2018**, *23*, No. 831.

(59) Sağlık, B. N.; Sen, A. M.; Evren, A. E.; Cevik, U. A.; Osmaniye, D.; Kaya Cavusoglu, B.; Levent, S.; Karaduman, A. B.; Ozkay, Y.; Kaplancikli, Z. A. Synthesis, investigation of biological effects and in silico studies of new benzimidazole derivatives as aromatase inhibitors. *Z. Naturforsch., C* **2020**, *75*, 353−362.

(60) Osmaniye, D.; Levent, S.; Sağlık, B. N.; Karaduman, A. B.; Özkay, Y.; Kaplancıklı, Z. A. Novel imidazole derivatives as potential aromatase and monoamine oxidase-B inhibitors against breast cancer. *New J. Chem.* **2022**, *46*, 7442−7451.

(61) Çevik, U. A.; Osmaniye, D.; Sağlik, B. N.; Çavuşoğlu, B. K.; Levent, S.; Karaduman, A. B.; Ilgin, S.; Karaburun, A. Ç.; Ozkay, Y.; Kaplancikli, Z. A.; Turan, G. Multifunctional quinoxaline-hydrazone derivatives with acetylcholinesterase and monoamine oxidases inhibitory activities as potential agents against Alzheimer's disease. *Med. Chem. Res.* **2020**, *29*, 1000−1011.

(62) Gençer, H. K.; Levent, S.; Acar Cevik, U.; Ozkay, Y.; Ilgin, S. New 1,4-dihydro[1,8]naphthyridine derivatives as DNA gyrase inhibitors. *Bioorg. Med. Chem. Lett.* **2017**, *27*, 1162−1168.

(63) Breivik, O. N.; Owades, J. L. Yeast Analysis, Spectrophotometric Semimicrodetermination of Ergosterol in Yeast. *J. Agric. Food Chem.* **1957**, *5*, 360−363.

(64) Levent, S.; Kaya Cavusoglu, B.; Saglik, B. N.; Osmaniye, D.; Acar Cevik, U.; Atli, O.; Ozkay, Y.; Kaplancikli, Z. A. Synthesis of Oxadiazole-Thiadiazole Hybrids and Their Anticandidal Activity. *Molecules* **2017**, *22*, No. 2004.

(65) Kaplancıklı, Z. A.; Levent, S.; Osmaniye, D.; Saglik, B. N.; Cevik, U. A.; Cavusoglu, B. K.; Ozkay, Y.; Ilgin, S. Synthesis and Anticandidal Activity Evaluation of New Benzimidazole-Thiazole Derivatives. *Molecules* **2017**, *22*, No. 2051.

(66) Can, N. O.; Acar Çevik, U.; Sağlık, B. N.; Levent, S.; Korkut, B.; Özkay, Y.; Kaplancıklı, Z. A.; Koparal, A. S. Synthesis, Molecular Docking Studies, and Antifungal Activity Evaluation of New Benzimidazole-Triazoles as Potential Lanosterol 14α-Demethylase Inhibitors. *J. Chem.* **2017**, *2017*, No. 9387102.

(67) Evren, A. E.; Nuha, D.; Dawbaa, S.; Saglik, B. N.; Yurttas, L. Synthesis of novel thiazolyl hydrazone derivatives as potent dual monoamine oxidase-aromatase inhibitors. *Eur. J. Med. Chem.* **2022**, *229*, No. 114097.

(68) Osmaniye, D.; Levent, S.; Sağlık, B. N.; Karaduman, A. B.; Ozkay, Y.; Kaplancikli, Z. A. Novel Imidazole Derivatives as Potential Aromatase and Monoamine Oxidase-B Inhibitors Against Breast Cancer. *New J. Chem.* **2022**, *46*, 7442.

(69) Acar Çevik, U.; Kaya Cavusoglu, B.; Saglik, B. N.; Osmaniye, D.; Levent, S.; Ilgin, S.; Ozkay, Y.; Kaplancikli, Z. A. Synthesis, Docking Studies and Biological Activity of New Benzimidazole- Triazolothia-diazine Derivatives as Aromatase Inhibitor. *Molecules* **2020**, *25*, No. 1642.

(70) Daina, A.; Michielin, O.; Zoete, V. SwissADME: a free web tool to evaluate pharmacokinetics, drug-likeness and medicinal chemistry friendliness of small molecules. *Sci. Rep.* **2017**, *7*, No. 42717.

(71) *Schrödinger Release 2020-3, Maestro*; Schrödinger, LLC: New York, NY, 2020.

(72) *Schrödinger Release 2020-3, Glide*; Schrödinger, LLC: New York, NY, 2020.

(73) *Schrödinger Release 2020-3: LigPrep 2020*; Schrödinger, LLC: New York, NY, 2020.

(74) *Schrödinger Release 2020-3, Desmond*; Schrödinger, LLC: New York, NY, 2020.

(75) Osmaniye, D.; Evren, A. E.; Saglik, B. N.; Levent, S.; Ozkay, Y.; Kaplancikli, Z. A. Design, synthesis, biological activity, molecular docking, and molecular dynamics of novel benzimidazole derivatives as potential AChE/MAO-B dual inhibitors. *Arch. Pharm.* **2022**, *355*, No. 2100450.